Review

Applications and Advantages of Atomic Layer Deposition for Lithium-Ion Batteries Cathodes: Review

Yury Koshtyal, Denis Olkhovskii [ID], Aleksander Rumyantsev and Maxim Maximov *[ID]

Institute of Metallurgy of Mechanical Engineering and Transport, Peter the Great Saint Petersburg Polytechnic University, 29, Polytechnicheskaja Street, 195251 Saint Petersburg, Russia
* Correspondence: maximspbstu@mail.ru

Abstract: Nowadays, lithium-ion batteries (LIBs) are one of the most convenient, reliable, and promising power sources for portable electronics, power tools, hybrid and electric vehicles. The characteristics of the positive electrode (cathode active material, CAM) significantly contribute to the battery's functional properties. Applying various functional coatings is one of the productive ways to improve the work characteristics of lithium-ion batteries. Nowadays, there are many methods for depositing thin films on a material's surface; among them, one of the most promising is atomic layer deposition (ALD). ALD allows for the formation of thin and uniform coatings on surfaces with complex geometric forms, including porous structures. This review is devoted to applying the ALD method in obtaining thin functional coatings for cathode materials and includes an overview of more than 100 publications. The most thoroughly investigated surface modifications are lithium cobalt oxide (LCO), lithium manganese spinel (LMO), lithium nickel-cobalt-manganese oxides (NCM), lithium-nickel-manganese spinel (LNMO), and lithium-manganese rich (LMR) cathode materials. The most studied processes of deposition are aluminum oxide (Al_2O_3), titanium dioxide (TiO_2) and zirconium dioxide (ZrO_2) films. The primary purposes of such studies are to find the synthesis parameters of films, to find the optimal coating thickness (e.g., ~1–2 nm for Al_2O_3, ~1 nm for ZrO_2, <1 nm for TiO_2, etc.), and to reveal the effect of the coating on the electrochemical parameters of batteries. The review summarizes synthesis conditions, investigation results of deposited films on CAMs and positive electrodes and some functional effects observed due to films obtained by ALD on cathodes.

Keywords: lithium-ion battery; cathode materials; atomic layer deposition; thin films; functional coatings; cyclic stability

1. Introduction

Lithium-ion batteries (LIBs), due to their high energy and power density, operability in a wide temperature range, and cycling life, are used for the autonomous power supply of portable devices, medical equipment, and electric and hybrid cars. However, LIBs' characteristics can be improved by using more advanced materials (active, inactive) and manufacturing technology.

One of the ways to improve performance characteristics is the application of thin functional coatings on materials and components of the LIB, which can not only ensure the safety of the battery material and safety of its use, but also improve such characteristics as specific energy and power by increasing the charging voltage, the discharge capacity, and increasing the electronic conductivity. For example, the doping of materials, applying a protective and ion-conductive coating (solid-state electrolyte, SSE) to lithium cobalt oxide allows for the upper charging voltage limit to be increased from 4.2 to 4.35 ÷ 4.45 V [1] without reducing the LIB's safety and cycling life. In addition, such expansion of the voltage interval increases the battery's specific energy, including by increasing the discharge capacity of the cathode material (a more significant fraction of atoms leaving/entering during charge-discharge).

Today, there are many methods of thin coating deposition on disperse and porous materials (sol-gel method [2], CVD [3], various kinds of sputtering, etc.). Atomic layer deposition (ALD, also known as molecular layer deposition, MLD) is usually preferred in the synthesis of especially thin coatings [4,5], due to it allowing the production of conformal coatings of a different chemical nature [6] with precise thickness control both on particles and on LIB components (positive and negative electrodes, separator). Furthermore, the use of specialized semi-periodic process reactors [7] makes it possible to modify a sufficiently large amount of material (hundreds of kilograms), e.g., the application of roll-to-roll technology [8] provides deposition on tapes (electrodes, separator). Thus, this method can also be implemented in manufacturing materials and electrodes.

The first attempts to improve the LIB using ALD were made relatively recently. To date, the method has been applied to the fabrication of thin-film positive [9–12] and negative electrodes [13–15], ionic conductors [16,17], thin-film LIB prototypes [18,19], separator modifications [20,21], negative [22–25] and positive electrodes materials [26–28] of traditional LIBs.

This review is devoted to applying atomic layer deposition in obtaining thin functional coatings on the surface of cathode materials. Articles for the analysis were obtained based on the Web of Science (WoS) search from 2010 to 2021 (inclusive). The following keywords were chosen: "cathode", "ALD", "Li-ion", and "coating". The first stage was the selection of articles based on the built-in machine search of the WoS database. Next, articles relevant to the topic of this review were selected based on an analysis of the information provided in the abstract. The distribution of the selected articles according to the year of publication, as well as the total number of citations per year, is illustrated in Figure 1a; the most frequently studied coatings on cathode materials are shown in Figure 1b.

(**a**)   (**b**)
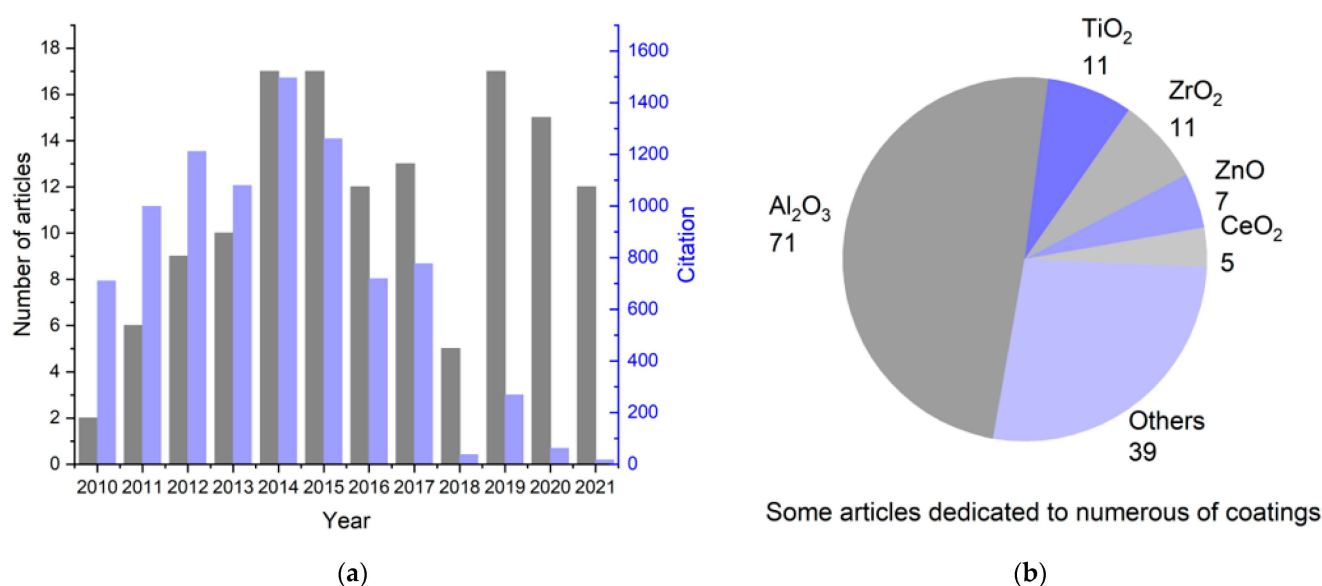
Figure 1. Summary statistics on the study of the literature about the synthesis of coatings on the cathode materials of lithium-ion batteries using ALD: (**a**) change in the number of publications related to ALD modification of cathode materials and their sum citation by year for 2010–2021; (**b**) number of articles devoted to a particular coating.

In this review, we will discuss the main results in the synthesis of coatings using the ALD method and their impact on the characteristics of positive LIB electrodes. Information on the physicochemical analysis methods used in cathode modifications with ALD can be found in Appendix A Table A1.

2. Synthesis of Functional Coatings on Cathode Materials by Atomic Layer Deposition

2.1. Functional ALD Coatings Used to Improve the Performance of Lithium-Ion Cathodes

Published studies to improve the performance of cathode materials and electrodes use Al_2O_3 [7,25,29–97], Al_2O_3:Ga_2O_3 [98], Al_2O_3-AlF_3 [87], AlF_3 [69,87,99,100], $AlPO_4$ [61,101,102], $AlPON$ [102], AlW_xF_y [103], CeO_2 [49,95,104–106], FeO_x [107–110], $FePO_4$ [111], HfO_2 [112], $LiAlO_2$ [48], $LiAlO_x$ [30], LiF [113], Li_3PO_4 [114], $LiTaO_3$ [115,116], $Li_xTi_y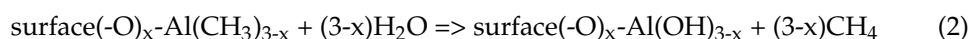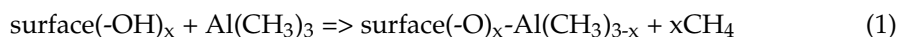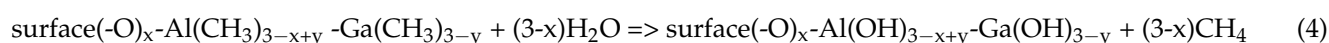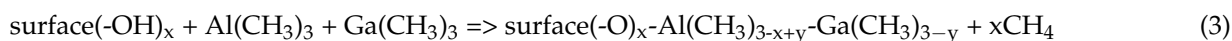O_z$ [117], MgO [44], MgF_2 [118], NbO_x [119], Ta_2O_5 [120], TiN [84,89], TiO_2 [7,30,31,33,45,47,65,121–124], TiO_x [117], TiO_2-ZnO [125], TiO_2-Li_3PO_4 [126], $TiPO_4$ [127], $TiPON$ [127], VO_x [128], ZnO [39,67,68,122,129–131], and ZrO_2 [30,44,45,49,67,68,132–136] coatings.

The synthesis of coatings according to the ALD method (MLD) is realized by sequential reactions between functional groups present on the solid surface and low-molecular reagents. Surface treatment processes with low-molecular reagents are separated by a stage of removing excess reagents and volatile reaction products by pumping out and/or purging the reaction space with gas (often nitrogen). To illustrate, we will give an example of one of the possible ways to obtain aluminum oxide films. By pumping and purging the reactor (vacuum chamber) with inert gas, the physically adsorbed water is removed from the surface of the cathode material (positive electrode) (Stage I). Then, trimethylaluminum vapor ($Al(CH_3)_3$—(Reagent A)) is introduced into the chamber (Stage II). Hydroxyl (functional) groups on the surface of the cathode material interact with the trimethylaluminum vapors (Reaction (1)), with the excess of Reagent A physically adsorbed on the surface of the modified material. To remove the excess of Reagent A, the chamber is evacuated and purged with inert gas (Stage III). The following introduction of water vapor (Reagent B) into the chamber (Stage IV) results in hydrolysis of the Al-CH_3 bond (Reaction (2)) with the formation of hydroxyl groups on the surface of the material. The excess water molecules are adsorbed on the surface of the modified material. To remove the water vapor, the chamber is evacuated and purged with inert gas (Stage V). Stages II–V form one cycle of coating synthesis. Cyclic treatment (repetition of Stages II-V) enables the growing of aluminum oxide coatings (these main stages are described in Figure 2).

$$surface(-OH)_x + Al(CH_3)_3 => surface(-O)_x\text{-}Al(CH_3)_{3\text{-}x} + xCH_4 \quad (1)$$

$$surface(-O)_x\text{-}Al(CH_3)_{3\text{-}x} + (3\text{-}x)H_2O => surface(-O)_x\text{-}Al(OH)_{3\text{-}x} + (3\text{-}x)CH_4 \quad (2)$$

Coatings incorporating more than two elements can be obtained using a mixture of low-molecular reagents. For example, by varying the vapor pressures of trimethylaluminum and trimethyl gallium (Reactions (3) and (4)) at the chemisorption stage (Stage II), one can set the aluminum to gallium ratio in the oxide coating [98]. Another way consists of a multistage treatment involving "sub-cycles". One cycle of $LiTaO_3$ film synthesis includes one "sub-cycle" of lithium oxide synthesis and six "sub-cycles" of tantalum oxide synthesis, each following the procedure described above (Stages I–V), using the corresponding low-molecular reagents (it can be noticed in tables below). Similar multistage treatment is performed when obtaining Al_2O_3-AlF_3 [87], $AlPO_4$ [61,101,102], $AlPON$ [102], $FePO_4$ [111], $LiAlO_2$ [48,137], $LiAlO_x$ [30,137], $Li_xTi_yO_z$ [117], MgF_2 [118], TiO_2-ZnO [125], TiO_2-Li_3PO_4 [126], $TiPO_4$ [127], and $TiPON$ [127] coatings. In the case of the synthesis of $LiAlO_x$ coatings, it is noted that an increase in the number of "sub-cycles" of lithium-containing layer deposition over 50% leads to a sharp increase in the mass of the grown coatings, which seems to be related to the inability to completely remove the physically adsorbed water in the synthesis' conditions.

$$surface(-OH)_x + Al(CH_3)_3 + Ga(CH_3)_3 => surface(-O)_x\text{-}Al(CH_3)_{3\text{-}x+y}\text{-}Ga(CH_3)_{3\text{-}y} + xCH_4 \quad (3)$$

$$surface(-O)_x\text{-}Al(CH_3)_{3\text{-}x+y}\text{ -}Ga(CH_3)_{3\text{-}y} + (3\text{-}x)H_2O => surface(-O)_x\text{-}Al(OH)_{3\text{-}x+y}\text{-}Ga(OH)_{3\text{-}y} + (3\text{-}x)CH_4 \quad (4)$$
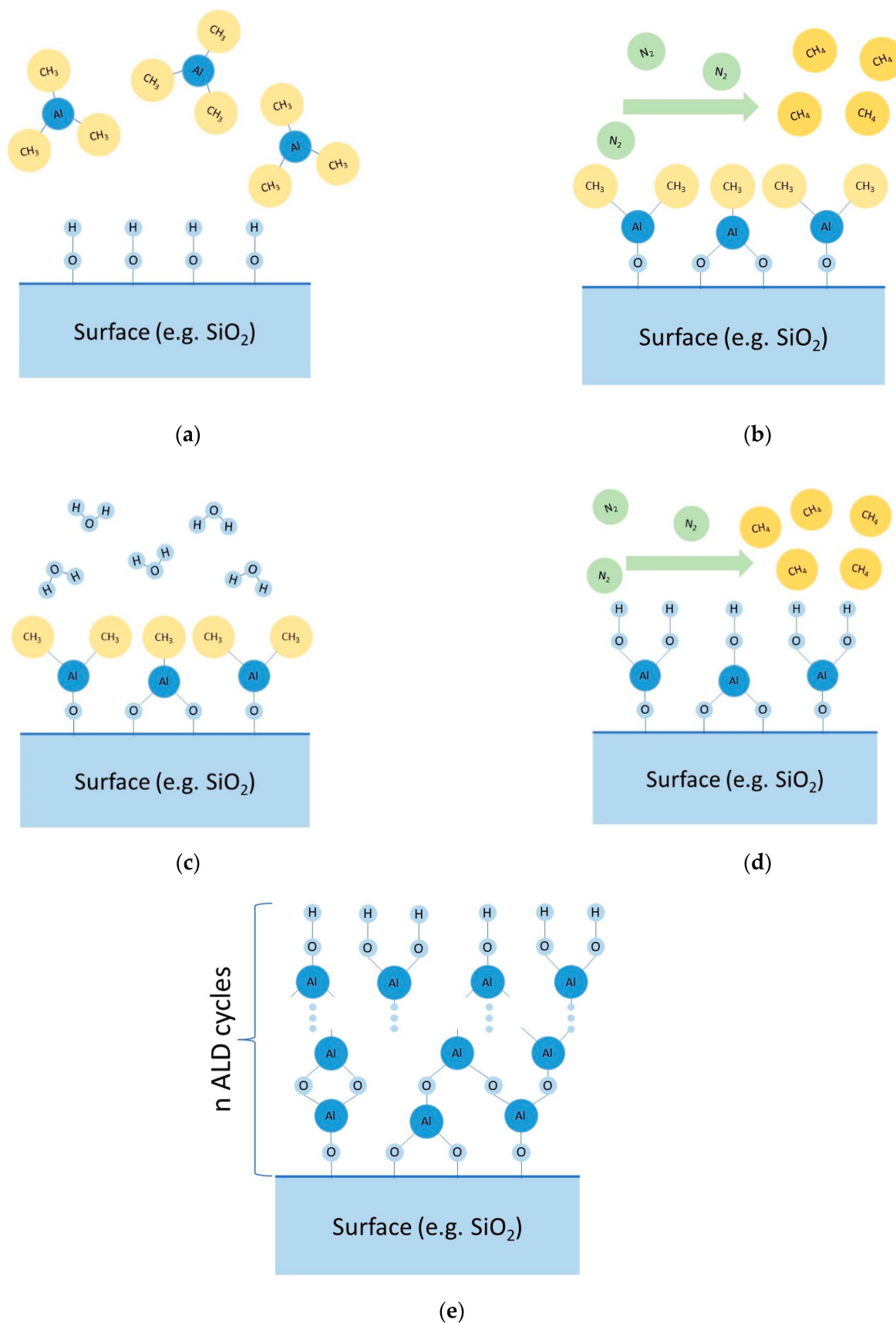
Figure 2. Principal scheme of main stages of ALD: (**a**) Stage II, (**b**) Stage III, (**c**) Stage IV, (**d**) Stage V, (**e**) future cycling.

Coating synthesis' parameters of different chemical compositions on electrodes and powders of cathode materials are reflected in tables: lithium cobalt oxide (LCO-LiCoO$_2$)—Table 1, lithium manganese spinel (LMO-LiMn$_2$O$_4$)—Table 2, lithium nickel-cobalt-manganese oxides (NCM) and lithium nickel-cobalt-aluminum oxides (NCA)—Table 3, lithium nickel-manganese spinel (LNMO–LiNi$_{0.5}$Mn$_{1.5}$O$_4$)—Table 4, lithium- and manganese-rich cathode materials with layered structure (LMR)—Table 5. However, due to a number of reasons (stable structure, carbon coating on industrial samples, low charging voltage, etc.), lithium iron phosphate LiFePO$_4$ rarely comes into the focus of scientists [84,89] trying to improve cathode materials using ALD technology. The effect of Al$_2$O$_3$ (obtained using TMA + H$_2$O at 177 °C—two, five and ten ALD cycles [89] and two, five and ten ALD cycles [84];) and TiN coating (obtained using TiN coating: TiCl$_4$ + NH$_3$ at 400 °C—five and ten ALD cycles [89] and five, ten and fifteen ALD cycles [84].). It was shown in [84] that modification during two (Al$_2$O$_3$) and ten (TiN) ALD cycles lead to the optimal performance of the materials.

Table 1. Main parameters of LCO (LiCoO$_2$) modification.

P/E	Coating	Reagent		T, °C (Time, h)	nC (Optimum)	Growth Per Cycle, Å/Cycle	Reference
		A	B				
P	Al$_2$O$_3$	TMA	H$_2$O	180	**2**, 6, 10, 20	2.2	[39]
		–	–	450 (10)	20	–	
		–	–	–	**2**, **4**, 6, 10	–	[58]
		TMA	H$_2$O	180	**2**, 25	≈2	[63]
		–	–	700 (4, 8,16)	25	–	
	ZnO	DEZ	H$_2$O	180	4	–	[39]
	ZrO$_2$	Zr(NMe$_2$)$_4$	H$_2$O	100	**2**	1.3	[45]
E	Al$_2$O$_3$	TMA	H$_2$O	180	**2**, 6, 10, 20	2.2	[39]
		TMA	H$_2$O	180	2, 20	–	[40]
		–	–	–	**2**, 6	≈2.5	[52]
		TMA	H$_2$O	150	**10**, 50, 100, 500	–	[31]
		TMA	H$_2$O	–	<10	1.1	[25]
		TMA	H$_2$O	150	**2**, 5, 10, 50	1.3	[45]
		TMA	H$_2$O	150	10, **20**, 30	–	[50]
		TMA	H$_2$O	180	30	≈1	[32]
		TMA	H$_2$O	180	2	–	[62]
		TMA	H$_2$O	150	2	–	[69]
	AlF$_3$	TMA	HF:Py	150	**2**, 5, 8	–	[69]
	AlW$_x$F$_y$	TMA	WF$_6$	200	4	2.56	[103]
	NbO$_x$	Nb(OEt)$_5$	H$_2$O	175	(15 nm, **30 nm**, 60 nm)	0.42	[119]
	TiO$_2$	TTIP	H$_2$O	150	10, **50**, 100, 500	–	[31]
		TTIP	H$_2$O	85	**2**	1.5	[45]
	ZrO$_2$	Zr(NMe$_2$)$_4$	H$_2$O	100	**2**	1.3	[45]

Footer. P—particles; E—electrode; nC—number of synthesis cycles; DEZ—diethyl zinc; HF:Py—hydrofluoric acid solution in pyridine; TMA—trimethylaluminum; TTIP—tetraisopropoxide titanium; Zr(NMe$_2$)$_4$—tetrakis(dimethylamido)zirconium.

Table 2. Main parameters of LMO (LiMn$_2$O$_4$) modification.

P/E	Coating	Reagent		T, °C (Time, h)	nC (Optimum)	Growth Per Cycle, Å/Cycle	Reference
		A	**B**				
P	Al$_2$O$_3$	TMA	H$_2$O	120	**6**, 50, 412	≈1.2	[46]
		TMA	H$_2$O	120	4, **6**, 8	1.5	[38]
		TMA	H$_2$O	120	6, 50	≈1.1	[67]
		TMA	H$_2$O	177	5	–	[49]
		TMA	H$_2$O	120	5 (0.19 nm), 10 (0.31 nm)	–	[73]
		TMA	H$_2$O	120	5 (0.6 nm), 10 (1 nm), 20 (1.7 nm)	–	[90]
		TMA	H$_2$O	177	5, 10 (1.5 nm), 25 (3 nm)	–	[95]
		TMA	H$_2$O	200	1	–	[96]
		TMA	–		1	–	
	CeO$_2$	Ce(iPrCp)$_3$	H$_2$O	250	10, 30, **50**, 100, 150	0.6	[49]
		Ce(iPrCp)$_3$	H$_2$O	250	(2, 3, 5 nm)	–	[105]
		Ce(iPrCp)$_3$	H$_2$O	250	30 (1.5 nm), 50 (3 nm), 100 (5 nm)	–	[95]
	ZnO	DEZ	H$_2$O	120	2, **6**, 10, 50	1.7	[131]
		DEZ	H$_2$O	120	**6**, 50	–	[129]
		DEZ	H$_2$O	120	6, 50	≈1.7	[67]
	ZrO$_2$	Zr(O(CH$_3$)$_3$)$_4$	H$_2$O	120	2, 6, 10, 50,300	–	[133]
		Zr(O(CH$_3$)$_3$)$_4$	H$_2$O	120	6, 50	2.9	[67]
		Zr(O(CH$_3$)$_3$)$_4$	H$_2$O	120	2, **6**, 10	≈2	[134]
		–	–	450 (3)	6	–	
		Zr(NMe$_2$)$_4$	H$_2$O	250	5	–	[49]
E	Al$_2$O$_3$	TMA	H$_2$O	120	4, **10**, 20	2	[37]
		TMA	H$_2$O	120	**6**, 50, 412	≈1.2	[46]
		TMA	H$_2$O	120	4, **6**, 8	1.5	[38]
		TMA	H$_2$O	120	6, 50	≈1.1	[67]
		TMA	H$_2$O	175	**10**, 50	≈1	[56]
		TMA	H$_2$O	100	1 nm	–	[47]
	TiO$_2$	TDMAT	H$_2$O	150	5 nm	–	
		TDMAT	H$_2$O	120	10, **15**, 40, 100	0.65	[123]
	ZnO	DEZ	H$_2$O	120	2, **6**, 10, 50	1.7	[131]
		DEZ	H$_2$O	120	**6**, 50	–	[129]
		DEZ	H$_2$O	120	6, 50	≈1.7	[67]
	ZrO$_2$	Zr(O(CH$_3$)$_3$)$_4$	H$_2$O	120	2, 6, 10, 50,300	–	[133]
		Zr(O(CH$_3$)$_3$)$_4$	H$_2$O	120	6, 50	2.9	[67]
–	Al$_2$O$_3$	TMA	H$_2$O	–	1	–	[92]

Footer. Ce(iPrCp)$_3$—Tris(cyclopentadienyl)cerium (III); TDMAT—tetrakis(dimethylamido)titanium.

Table 3. Main parameters of NCM and NCA ($LiNi_{0.8}Co_{0.15}Al_{0.05}O_2$) modification.

(XYZ)	P/E	Coating	Reagent		T, °C (Time, h)	nC (Optimum)	Growth Per Cycle, Å/Cycle	Reference
			A	B				
(111)	P	Al_2O_3	TMA	H_2O	–	**2**, **_4_**, 6, 10	2.2	[51]
			TMA	H_2O	180	4	1.3	[71]
			–	–	300 (12)	–	–	[71]
			TMA	H_2O	120	2, 4 (1 nm), 6, 7, 10, 12, 15 (3–3.2 nm)	2.2	[81]
	E	Al_2O_3	TMA	H_2O	85	8, 15, 30 (≈3 nm), 60, 100	0.99	[94]
		$LiTaO_3$	1× LiO^tBu	H_2O	225	2, **5**, **_10_**, 20	≈2.5	[115]
			6× $Ta(OEt)_5$	H_2O	225			
(424)		Al_2O_3	TMA	H_2O	120	4	1.1–1.5	[57]
(523)	P	Al_2O_3	TMA	H_2O	200	5	1.2	[44]
			TMA	H_2O	180	2, 8	–	[80]
			TMA	H_2O	100	5	1	[91]
		Al_2O_3-Ga_2O_3	TMA, TMG	H_2O +O_3	200	**2**, **5**	0.9–1.1	[98]
		AlF_3	TMA	TaF_5	125	5	–	[99]
		MgO	$Mg[EtCp]_2$	H_2O	200	5	1.4	[44]
		ZnO	DEZ	H_2O	100	8	≈1.7	[130]
		ZrO_2	$Zr(NMe_2)_4$	H_2O	150	2, **5**, 8	1.9	[132]
			$Zr(NMe_2)_4$	H_2O	200	5	0.8	[44]
	E	Al_2O_3	TMA	H_2O	120	2, **_5_**, 8, 10	1.0–3.0	[55]
			TMA	H_2O	180	2, **_4_**, 8, 15	1.1	[53]
		Ta_2O_5	$Ta(OEt)_5$	H_2O	200	2, **_5_**, 10	0.8	[120]
		TiO_2	TTIP	H_2O	120, 150, 180	≈100	–	[124]
(622)	P	Al_2O_3	TMA	H_2O	110	4 (0.5 nm), 10 (1.3 nm), 40 (5.3 nm)	≈1.3	[85]
		Al_2O_3	TMA	H_2O	100	10 (≈1 nm), **_20_** (**_≈ 2 nm_**), 40 (≈4 nm)	≈1.1–1.2	[74]
		$AlPO_4$	1× TMPO	O_{2pl}	–	2 (≈1 nm)	–	[102]
			1× TMA					
		AlPON	1× DEPA	N_{2pl}	–	1 (≈1 nm), (20 nm)	–	[102]
			1× TMA					
		TiO_2	$TiCl_4$	H_2O	200	139	0.36	[121]
		$TiPO_4$	TMPO	TTIP	–	–	–	[127]
			O_{2pl}					
		TiPON	DEPA	TTIP	–	(2 nm)	6	[127]
			N_{2pl}					
		ZrO_2	$Zr(NMe_2)_4$	H_2O	150	2, 5 (≈1.2 nm), 8, 50	–	[136]
	E	Al_2O_3	TMA	H_2O	120	5	1	[97]

Table 3. *Cont.*

(XYZ)	P/E	Coating	Reagent		T, °C (Time, h)	nC (Optimum)	Growth Per Cycle, Å/Cycle	Reference
			A	**B**				
(622)	E	$Li_xTi_yO_z$	$4\times$ TTIP	H_2O	200	10	1.8	[117]
			$1\times$ LiO^{t}Bu	H_2O				
		TiO_x	TTIP	H_2O	200	50	0.33	[117]
		ZrO_2	$Zr(NMe_2)_4$	H_2O	100	5 (0.8 nm), **20** (**≈3.2 nm**), 40 (6.5 nm)	1.62	[135]
FCG (713)	P	Al_2O_3	TMA	–	180	(1 nm)	–	[76]
(811)		Al_2O_3	TMA	H_2O	150	**2**, 5, 10	–	[86]
			TMA	H_2O	120	10, **20** (**2.2 nm**), 50 (5.6 nm)	1.12	[88]
			TMA	H_2O	100	10 (≈3.4 nm)	–	[75]
			TMA	H_2O	–	–	–	[93]
	E	Al_2O_3	TMA	H_2O	120	5	1	[97]
FCG (811)	P	Al_2O_3	TMA	H_2O	–	–	–	[7]
NCA		TiO_2	$TiCl_4$	H_2O	–	–	–	
FCG (1011)		Al_2O_3	TMA	H_2O	150		–	[72]
(851005)		HfO_2	TEMAH	O_3	250	20	0.43	[112]
(71575)	E	Al_2O_3	TMA	H_2O	120	5	1	[97]

Footer. (XYZ)—the ratio of Ni:Co:Mn (X:Y:Z) in the formula $LiNi_{x/(x+y+z)}Co_{y/(x+y+z)}Mn_{z/(x+y+z)}O_2$; FCG—cathode material with gradient of element concentration in secondary particles ($LiNi_{0.68}Mn_{0.22}Co_{0.10}O_2$, $LiNi_{0.77}Mn_{0.11}Co_{0.12}O_2$, $LiNi_{0.83}Mn_{0.05}Co_{0.12}O_2$); Mg[EtCp]$_2$ – bis(ethylcyclopentadienyl)magnesium; Ta(OEt)$_5$—tantalum (V) ethoxide; TMG—trimethyl gallium; 1x, 4x, 6x (and others)—1, 4, 6 (and others) synthesis' sub-cycles; TMP—trimethyl phosphate plasma; DEPA—diethylphosphoramidate plasma; TEMAH—$Hf[N(CH_2CH_3)(CH_3)]_4$.

Table 4. Main parameters of LNMO ($LiNi_{0.5}Mn_{1.5}O_4$) modification.

P/E	Coating	Reagent		T, °C (Time, h)	nC (Optimum)	Growth Per Cycle, Å/Cycle	Reference
		A	**B**				
P	Al_2O_3	TMA	H_2O	250	**5**, 10, 15, 30	≈0.8	[33]
		TMA	H_2O	180	0, 2, **4**, 6, 10	2	[41]
		TMA	H_2O	225	5	–	[42]
	AlF_3	$1\times$ TMA	O_3	150	2 (≈2.4 nm), 4 (≈4.6 nm)	–	[100]
		$1\times$ Hfac	O_3				
		$1\times$ TMA	O_3	240	2	–	
		$1\times$ Hfac	O_3				
	CeO_2	$Ce(iPrCp)_3$	H_2O	250	30, 40, **50**, 70, 100	0.6	[104]
	FeO_x	$FeCp_2$	O_2	450	10, 20, 25, **30**, 40, 80, 160	0.2	[107]

Table 4. *Cont.*

| P/E | Coating | Reagent | | T, °C (Time, h) | nC (Optimum) | Growth Per Cycle, Å/Cycle | Reference |
		A	B				
P	FeO$_x$	FeCp$_2$	O$_2$	450	50	–	[108]
		FeCp$_2$	O$_2$	450	–	–	[110]
	FePO$_4$	1× FeCp$_2$	O$_3$	300	5, **10**, 20, 40	1	[111]
		1× (CH$_3$)$_3$PO$_4$	H$_2$O				
	MgF$_2$	1× Mg[EtCp]$_2$	O$_3$	275	4, 6, **12**	0.65, 0.59, 0.48	[118]
		1× Hfac	O$_3$				
	LiF	LiO^{t}Bu	Hfac	220	4	–	[113]
		LiO^{t}Bu	TiF$_4$			–	
	Li$_3$PO$_4$	LiO^{t}Bu	TMPO	250	–	–	[126]
	TiO$_2$	TiCl$_4$	H$_2$O	250	**11**, 15, 30, 50	≈0.4	[33]
		TTIP	H$_2$O	250	–	–	[126]
	TiO$_2$-Li$_3$PO$_4$	TTIP	H$_2$O	250	**10 (1 nm)**, 50 (5 nm)	–	[126]
		LiO^{t}Bu	TMPO				
E	Al$_2$O$_3$	TMA	H$_2$O	90	3, **10**, 30	1.2	[35]
		–	–	–	0.55–5 nm	–	[60]
		TMA	H$_2$O	150	**4**, 6	1	[54]
		TMA	H$_2$O	90	10	1.2	[36]
		TMA	H$_2$O	–	2, 5,10	–	[48]
	AlPO$_4$	1× TMPO	H$_2$O	250	2, 5, **10**, 20, 50	–	[101]
		1× TMA	H$_2$O				
	LiAlO$_2$	1× TMA	H$_2$O	225 [137]	5, 10	–	[48]
		1× LiO^{t}Bu	H$_2$O				
	Li$_3$PO$_4$	TMPO	LiO^{t}Bu	300	17 (1 nm), 50 (3 nm), 83 (5 nm)	0.6	[114]

Footer. FeCp$_2$—ferrocene; Hfac—hexafluoroacetylacetone; LiO^{t}Bu—lithium t-butoxide; TMPO—(MeO)$_3$PO.

Table 5. Main parameters of LMR modification.

| Mt | P/E | Coating | Reagent | | T, °C (Time, h) | nC (Optimum) | Growth Per Cycle, Å/Cycle | Reference |
			A	B				
L1	P	Al$_2$O$_3$	TMA	H$_2$O	180	2, **6**, 20	–	[70]
			TMA	H2O	150	10	2–3	[65]
			TMA	H$_2$O	120	6	–	[68]
			TMA	H$_2$O	150	20	–	[61]
		AlPO$_4$	1× TMA	H$_2$O	250	5, 10, 20	2	[61]
			1× (CH$_3$)$_3$PO$_4$	H$_2$O				
		TiO$_2$	TTIP	H$_2$O	150	20	<2	[65]
		ZnO	DEZ	H$_2$O	120	2, 6, 10	≈1.9	[68]
		ZrO$_2$	Zr(O(CH$_3$)$_3$)$_4$	H$_2$O	120	**6**	≈1.3	

Table 5. *Cont.*

| Mt | P/E | Coating | Reagent | | T, °C | nC | Growth Per | Reference |
			A	B	(Time, h)	(<u>Optimum</u>)	Cycle, Å/Cycle	
		Al₂O₃	TMA	H₂O	180	2, **6**, 20	−	[70]
			−	−	300 (3)	2, **6**, 20	−	
			TMA	H₂O	150	10, 20	−	[43]
	E		TMA	H₂O		2, 4, 6	−	
		Al₂O₃-AlF₃	1× TMA	HF			−	
			5× TMA	H₂O	100			[87]
		Al₂O₃-AlF₃	2× TMA	HF		1	−	
			4× TMA	H₂O				
		Al₂O₃-AlF₃	4× TMA	HF			−	
			2× TMA	H₂O				
L1	E	Al₂O₃-AlF₃	5× TMA	HF	100	1	−	[87]
			1× TMA	H₂O				
		AlF₃	TMA	HF		2, 4, 6, 8	−	
		Al₂O₃	TMA	H₂O	80	0, 0.5, 1.2, **<u>3.4 nm</u>**	−	[29]
			TMA	H₂O	120	5, 100	−	
		LiAlOₓ	TMA	H₂O	−	6	−	
L2	E		LiOᵗBu	H₂O	−	6	−	[30]
		TiO₂	TTIP	H₂O	100	6	−	
			TTIP	H₂O	150	6	−	
		ZrO₂	Zr(NMe₂)₄	H₂O	100	6	−	
			Zr(NMe₂)₄	H₂O	150	6	−	
L3	E	Al₂O₃	TMA	O₂	100	5, 10	−	[34]
	P	Al₂O₃	TMA	H₂O	−	4	≈2.5	[66]
			TMA	H₂O	150	4	−	[64]
		TiO₂	TiCl₄	H₂O	100	10	≈1.5	[122]
		TiO₂-ZnO	6× TiCl₄	H₂O	100			
			4× DEZ	H₂O	150			
L4		TiO₂-ZnO	4× DEZ	H₂O	150			
	E		6× TiCl₄	H₂O	100	(1.7 nm)	−	[125]
		TiO₂-ZnO	3× TiCl₄	H₂O	100			
			4× DEZ	H₂O	150			
			3× TiCl₄	H₂O	100			
		ZnO	DEZ	H₂O	150	5	≈3	[122]
L5	P	Al₂O₃	TMA	−	200	50	−	[79]
L6	P	FeOₓ	FeCp₂	O₂	450	20, 40, 100, 150	−	[109]
L7	P	Al₂O₃	TMA	H₂O	200	16, **<u>24</u>**, 40	−	[82]
L8	P	Al₂O₃	TMA	H₂O	−	−	−	[78]

Table 5. *Cont.*

Mt	P/E	Coating	Reagent		T, °C (Time, h)	nC (Optimum)	Growth Per Cycle, Å/Cycle	Reference
			A	**B**				
L9	P	–	–	–	–	–	–	[83]
L10	–	$LiTaO_3$	$1\times$ LiO^{t}Bu	H_2O	235	2, 5, 10 ($\approx$3 nm), 20	–	[116]
			$6\times$ Ta(OEt)$_5$	H_2O				
–	P	Al_2O_3	TMA	H_2O	150	**10**, 20, 40	–	[77]

Footer. Mt—types of materials such as: L1—$Li_{1.2}Mn_{0.54}Ni_{0.13}Co_{0.13}O_2$; L2—$Li_{1.2}Ni_{0.15}Mn_{0.55}Co_{0.1}O_2$; L3—$0.3Li_2MnO_3 + 0.7LiMn_{0.60}Ni_{0.25}Co_{0.15}O_2$; L4—$Li_{1.2}Ni_{0.2}Mn_{0.6}O_2$; L5—$0.35Li_2MnO_3+0.65LiNi_{0.35}Mn_{0.45}Co_{0.20}O_2$; L6—$Li_{1.13}Mn_{0.54}Ni_{0.13}Co_{0.14}O_2$; L7—$Li_{1.2}Ti_{0.4}Mn_{0.4}O_2$; L8—$Li_{1.2}Ni_{0.16}Mn_{0.56}Co_{0.08}O_2$; L9—$Li_{1.33}Ni_{0.27}Mn_{0.60}Co_{0.13}O_{2+d}$; L10—$Li_{1.13}Mn_{0.577}Ni_{0.256}Co_{0.097}O_2$.

2.2. Substantiation of the Synthesis Parameters and Reagents Choice

The stability of the binder and reagents determines the upper-temperature limit of coatings deposition. The minimum temperature of modifying electrodes with polyvinylidene fluoride (PVDF) binder was 120 °C [97,123]. The maximum modification temperatures of the electrodes with PVDF and polytetrafluoroethylene were 180 °C [53] and 300 °C (annealing temperature in the air after synthesis) [70], respectively. The maximum coatings' synthesis temperature on cathode particles was 450 °C (Al_2O_3 [37], FeO_x [107–110], ZrO_2 [84]) and 700 °C (Al_2O_3 [61]), the annealing temperature reached 700 °C [63,91,108–110,136]. One article mentions cathode material (NCM851005) holding at 750 °C in an oxygen atmosphere before the synthesis of HfO_2 coating [112].

In some cases, atomic layer deposition is given a particular preference because of the possibility of low-temperature synthesis. For instance, authors of articles [97,123] argue the need for positive electrode modification at 120 °C because of the decomposition of PVDF at elevated temperatures.

Apparently, the choice of organometallic compounds in the role of Reagent A is due to the lack of a release of corrosive reaction products and the ability to enter into hydrolysis reactions. However, the drawback of these reagents is a carbon trace in the deposited films [96]. Water is used as a Reagent B, more rarely oxygen, or ozone is applied to obtain oxide films. Synthesis of fluorine-containing coatings is performed using WF_6 [103], TaF_5 [99], TiF_4 [113], hexafluoroacetylacetone [100,113,118] and hydrofluoric acid solution in pyridine [69,87]. For the syntheses phosphate coatings, as Reagent B usually uses trimethylphosphate [61,101,102,111,114,126,127] and diethylphosphoramidate [102,127].

In cases where high energy is required to activate the ALD process, plasma of metal-organic compounds [102,127], nitrogen [102,127], oxygen, etc. can be used as reagents. In works [102,127], the effect of using plasma of metal-organic compounds on the process course of atomic layer deposition is investigated. It is noted that the use of metal-organic plasma is most effective at lower synthesis temperatures [102,127] because the plasma polymerization of the reagents decreases with increasing substrate temperature, which reduces the growth of film thickness per ALD cycle. The authors also show that the use of several plasma reagents (metal-organic and nitrogen plasma) to produce nitrogen-doped coatings is much more effective in terms of thickness increment per ALD cycle, which can be caused by the increased carbon content in the films [102,127].

2.3. Synthesis of Specific Fluoride Coatings

In the synthesis of aluminum fluoride AlF_3 coatings, various impurities in the coating composition indicate the course of side reactions. A transmission electron microscopy (TEM) study of AlF_3 coatings obtained using $Al(CH_3)_3$ и WF_6 as reagents revealed tungsten-containing inclusions (tungsten metal and/or tungsten carbide) [103]. The formation of these inclusions provided an increase in the electronic conductivity of the coating.

Based on X-ray photoelectron spectroscopy (XPS) studies of the AlF3, coating deposited with trimethylaluminum and tantalum (V) fluoride, the presence of AlO_xF_y and

Ta_2O_5 compounds were found [99]. One possible reason for the oxygen appearance in the composition of the coatings may be the interaction of $-AlF_n$ and $-TaF_m$, groups with water vapor as a result of contact with the air atmosphere. The presence of tantalum in the composition of the films may be due to incomplete removal in the process of desorption (Stage III) of weakly volatile compounds of the composition $TaF_{5-x}(CH_3)_x$. It was found that the concentration of tantalum in the coating composition obtained on the lithiated nickel-cobalt-manganese oxide (12 at.%) is higher than on the silicon oxide layer (4–5%). The detected difference in the tantalum impurity content may be due to the different distribution and reactivity of hydroxyl groups on the surface of the cathode material (Ni-OH, Co-OH, Mn-OH) and the silicon oxide film (Si-OH). The presence of lithium-containing impurities on the surface of the cathode material can also have an influence.

An alternative way to obtain purer AlF_3 coatings is using trimethylaluminum and Olach's reagent (70% hydrogen fluoride solution in pyridine) [69,87,138]. The peculiarity of the growth mechanism is that after treatment with the vapor of Olach's reagent and the following stage of desorption, a monolayer of hydrogen fluoride molecules is present on the surface along with the fluoride functional groups. The interaction of trimethylaluminum occurs with hydrogen fluoride molecules, and as the cyclic treatment proceeds, a structural rearrangement occurs with the formation of the AlF_3 phase [138]. In an XPS study of the AlF_3, film deposited on a silicon wafer, it was recorded that regardless of the sputtering profile depth, approximately 2 at.% oxygen was detected in the coating composition. The authors attribute the presence of oxygen in the composition of the synthesized coating to the possible presence of water vapor formed as a result of interaction between hydrogen fluoride and the oxide film of the metal reactor body [138]. Hydrogen fluoride can also interact with the surface of the cathode material. When studying using XPS electrodes of lithiated cobalt oxide after cyclic treatment with trimethylaluminum vapor and Olach's reagent, along with a maximum in the 685.2 eV region characteristic of AlF_3, a maximum in the 682.2 eV region was found, indicating the possible formation of Co-F or Li-F bonds [69].

In paper [113], LiF films obtained using the two precursors TiF_4 and hexafluoroacetylacetone were studied. XPS analysis showed that when lithium fluoride was grown using the organic precursor, an additional peak in the F1s region was observed, characterizing the CF_x bonding energy. The authors suggested that during the synthesis of a LiF coating, using a metal-organic precursor in the film leaves unreacted organic radicals of a large size, resulting in the formation of numerous pores in the volume of the coating. These pores manifest themselves as additional diffusion channels for lithium ions through the coating material during electrochemical tests.

2.4. Evaluation of the Uniformity of the Grown Coatings

In a study using SEM and TEM of cathode powders coated with Al_2O_3 (2 and 3 cycles [80], 1–4 nm [85], 50 cycles [86], 20 cycles [88], 20 cycles [90], 5 cycles [97]), $AlPO_4$ (20 cycles [61], 50 cycles [101]), CeO_2 (100 cycles [95]), HfO_2 (20 cycles [112]), Me_xO_y и MeF_x [139], Ta_2O_5 (5 cycles [120]), TiO_2 (139 cycles [121], 10 cycles [122], 100 cycles [123]), ZnO (50 cycles [129]), ZrO_2 (50 cycles [134], 20 cycles [135]) coating elements were found that uniformly distributed over the particle surface. In this regard, it can be concluded that the coating deposition during cathode material particle modification is quite uniform.

LIB positive electrode is an aluminum foil with a porous solid active mass (about 100 μm thick) consisting of particles of active cathode material (84–95 wt.%), conductive additive (carbon black, conductive graphite 2–10 wt.%), and binder (PVDF, fluoroplastic, latex 3–8 wt.%). Uniformity of chemical elements distribution over the electrode active mass surface of ALD coated electrodes was demonstrated by means of SEM- and TEM-EDX studies of electrodes modified with Al_2O_3 (3.4 nm [29], 30 cycles [35], 10 cycles [36], 2–50 cycles [45], 1 nm [76], 24 cycles [82], 50 cycles [86], 20 cycles [88], 1 nm [77], 50 cycles [79], 10 cycles [75], 2 and 3 cycles [80], 20 cycles [90], 20 cycles [74], 30 cycles [94], 5 cycles [97]), $AlPO_4$ (20 cycles [101]), $LiTaO_3$ (2-20 cycles [115], 10 cycles [116]), $Li_xTi_yO_z$ (10 cycles [117]), TiO_2 (2–50 cycles [45], 10 cycles [122], 100 cycles [123]), TiO_x (50 cycles [117]), TiO_2-ZnO (10 cy-

cles [125]), TiO_2-Li_3PO_4 (5 nm after electrochemical studies [126]), ZnO (50 cycles [129], 5 cycles [122]) and ZrO_2 (2–50 cycles [45], 20 cycles [135]). It was also shown [35], that the elements of the modifying coating are also uniformly distributed over the cross-section of the electrode's active layer. Considering the above, we can conclude that the atomic layer deposition allows for uniform (at the micro level) coatings growth both on the particles of cathode powders and in the porous space of electrodes. On the other hand, the results of a study [64] using the TEM of the element (Al) coating (Al_2O_3) distribution of $Li_{1.2}Mn_{0.6}Ni_{0.2}O_2$ particles show that in addition to uniformly coated particles, there may be particles not completely coated [64]. It was shown that with increasing Al_2O_3 layering cycles of NMC111 particles, the transition metals Ni, Mn, and Co are coated with aluminum oxide to a greater extent, while Li particles are coated to a lesser extent by the film [81]. Thus, at the nano level, the uneven distribution of coating is possible.

2.5. Modification of Cathodes and Electrodes with Different Functional Groups on the Surface

During the modification of positive LIB electrodes, low molecular reagents can interact not only with the hydroxyl groups of the cathode material. In a study [29] of positive electrodes based on the cathode material $Li_{1.2}Mn_{0.54}Ni_{0.13}Co_{0.13}O_2$, it was found that with the increase of aluminum oxide coating thickness from 0 to 3.4 nm, a decrease in the intensity of O1s (529.6 eV—$Li_{1.2}Mn_{0.54}Ni_{0.13}Co_{0.13}O_2$) and C1s (284.6 eV—carbon black Super P, 285.0 eV—conductive graphite) bands is observed. The C1s (286.4 eV—C-H (PVDF), 290.9 eV—C-F (PVDF)), and F1s (687.8 eV—PVDF) peaks decrease in intensity and shift toward lower binding energies. A new maximum appears in the region of 685.5 eV, characterizing the presence of compounds with the composition AlO_xF_y. Taking into account the changes in the XPS spectra, the authors concluded that aluminum oxide covers the cathode material, conductive additives, and binder. The shift of the maxima characteristic of the binder—C1s and F1s may indicate the doping of the binder. On the other hand, during studying of TiO_2 films deposition on $LiMn_2O_4$ [123], it was found that due to the hydrophobic selectivity of the PVDF binder, the coating prioritizes growth on the surface of the active cathode material and carbon black (Super P), which also has its hydroxyl groups. Based on the shift of the O1s peaks (from 529.6, 530.6 eV to 529.2, 529.8 eV), C-O (from 531.5, 532.3, 533.4 eV to 531, 532.2, 533.1 eV) and Al2p deconvolution (73.6 and 74. 5 eV) when coating NMC111 with Al_2O_3 film, the authors of paper [94] suggest the possibility of the formation of an aluminum solid solution on the surface of NMC111 ($Li_{1+x}Ni_aMn_bCo_cAl_yO_2$, where a, b and c are close to 0.33), although it is also noted that the presence of peaks of 74.5 eV and 529.8 eV may also indicate the formation of Al-O bond.

During the synthesis of AlF_3 coatings, an additional maximum (685.0 eV) characterizing the presence of lithium fluoride on the surface of the modified cathode was observed in the XPS spectra of the obtained samples [87]. The presence of lithium fluoride on the surface of the modified samples may indicate the interaction of fluorine-containing precursors with the cathode material or with the lithium-containing impurities ($LiOH$, Li_2CO_3) present on the cathode material surface.

Since the chemical reactions, as a rule, proceed with the participation of surface hydroxyl groups, the coating growth process by the ALD does not change the structure of the material bulk. However, there are descriptions in the literature of cases when the growth process affects the phase [61] and chemical [107] composition of the bulk or near-surface layers [64] of cathode material particles. In a study using X-ray absorption spectroscopy, it was found that during the process of coating $AlPO_4$ on the cathode material $Li_{1.2}Mn_{0.54}Ni_{0.13}Co_{0.13}O_2$, some manganese atoms (17.8%) and cobalt (15.5%) are reduced to an oxidation degree of +2. The appearance of the spinel phase in the outer layers of the modified cathode material was also established using TEM. The degree of reduction in some of the atoms leads to a local transformation of the crystal structure near the surface of the cathode material.

A TEM study of lithium nickel-manganese spinel particles after 160 cycles of treatment with $FeCp_2$ vapor and oxygen has shown [107] that a conformal, thin (3 nm) FeO_x coating is present on the particle surface. Furthermore, when analyzing the chemical composition of the cross-section of modified cathode material particles using energy dispersive X-ray spectroscopy, it was found that iron atoms were present in bulk, the concentration of which decreased with distance from the outer surface. The presence of atoms in the bulk of the cathode material is probably due to the accelerated diffusion of iron atoms due to the synthesis at high temperature (450 °C). The diffusion of atoms from deposited coating were also observed while studying TiN deposition on $LiFePO_4$ [89]. Some Ti^{4+} ions diffuse into the material depth and occupy the Li^+ vacancies in the coating process. Doping $LiFePO_4$ with titanium atoms reduced the polarization of the cathode. In the presence of TiN coating on the cathode during cyclic charge-discharge, along with the change in iron oxidation degree (Fe^{3+}/Fe^{2+}), the Ti^{4+}/Ti^{3+} reaction was observed on the CV curves (peaks at 2.29, 2.42, 2.80 and 3.45 V).

2.6. Effect of Heat Treatment on Cathode Materials with Coatings

The introduction of atoms from coatings into the outer layers of the cathode material can be achieved by heating at elevated temperatures. In a recent study [63], the XPS spectra of aluminum oxide coated (25 cycles) particles of lithiated cobalt oxide were compared without heating and after annealing at 700 °C for 16 h. It was found that the position of $Co2p_{1/2}$ (780.5 eV) and O1s (532.2 eV) maxima did not change after two synthesis cycles, testifying the absence of influence of aluminum oxide coating on the outer layers of lithiated cobalt oxide particles. Thermal treatment resulted in a shift of $Co2p_{1/2}$ and O1s maxima positions to high energies to about 783 eV and 533.2 eV, and $Al2p_{3/2}$ maxima to lower energies to 73.3 eV. Thermal treatment resulted in a shift of the positions of $Co2p_{1/2}$ and O1s maxima to high energies to about 783 eV and 533.2 eV, and $Al2p_{3/2}$ maxima to lower energies to 73.3 eV. Considering that the value of the maximum $Al2p_{3/2}$ for the heated sample is close in position characteristic of $LiAlO_2$, but higher than that of the compound $LiCo_{0.9}Al_{0.1}O_2$, and increasing lattice parameters (a, c) the authors have suggested the formation of an alloy $LiAl_xCo_{1-x}O_2$ (where $0 < x < 0.1$).

After deposition of Al_2O_3 films on the NMC532 cathode material, annealing at different temperatures (100, 300, 500, and 700 °C) was performed [91]. Based on the XPS results, it was found that increasing the annealing temperature negatively affects the position of the Al2s peaks: a linear decrease in the aluminum binding energy is observed with increasing temperature, which leads to a decrease in the alumina phase in the coating and an increase in the metallic aluminum phase (based on the tabulated values). It was concluded that at high temperatures, the character of aluminum bonds changes from ionic to covalent. The Al/Co ratio decreases nonlinearly with increasing temperature, probably due to aluminum diffusion into the cathode bulk, which contributes to forming solid solutions.

In a study using XPS of electrodes modified with aluminum oxide (6 cycles) [68], it was found that as a result of heating at 300 °C the atomic ratios M/Al (M = Mn, Ni, Co) increase. Thus, the diffusion of aluminum atoms from the modifying coating (aluminum oxide) into the cathode material by forming the $Li_{1+x}Al_{1-y}M_yO_2$ phase is possible at sufficiently low temperatures. A similar conclusion was made during LCO modification by niobium oxide film [119]. A shift and change in the intensities of Nb4s, Li1s, $Nb3d_{3/2}$, and O1s peaks were observed during annealing at 700 °C. The observed changes are attributed to the effect of the annealing process not only in the modified surface but also in the cathode material, causing diffusion of Li and its binding with the oxygen of the surface layer.

To improve the cycling life of the cathode materials due to increment of Li diffusion, the NMC622 cathodes coated with ZrO_2 were annealed at different temperatures: 300, 500, and 700 °C [136]. The SEM studies of annealed samples showed that with an increase of the heat treatment temperature up to 700 °C, the cathode's morphology changes markedly, namely, the formation of nanoparticle islands, which increase the surface roughness, are observed. Additional TEM and EDX studies revealed that these nanoparticles consist only

of Zr and O (transition metals were not detected in the composition), and the interplanar distance is 0.285 nm. Therefore, it was suggested that a monoclinic phase of Li_2ZrO_3 with plane (111) was formed on the surface. Furthermore, with the increase in annealing temperature, the decrease in $Zr3d_{3/2}$ и $Zr3d_{5/2}$ bond energies are observed. Thus, the cathode is doped with Zr^{4+} ions. The doping presumably occurs in the Li and Ni sites (at 700 °C, part of Zr remains on surface with formation of new Li_2ZrO_3 phase), also with the increase in annealing temperature because of doping with Zr^{4+} ions, an increase in Ni^{2+} ions concentration and a decrease in Ni^{3+} ions concentration is observed.

In study [109], authors found an increase in capacity (in the first cycles by 2–4%) and an increase in the diffusion coefficient of materials annealed at 700 °C after modification with iron oxide (FeO_x) as compared to modified samples without annealing. Similar patterns were noted in [108]. Such an effect of annealing is explained by iron doping of the spinel structure, which results in electron density redistribution and slight changes in the spinel structure parameters. It was found that the diffusion coefficient of lithium ions in coated and annealed LNMO is 100 times higher than in pure LNMO [108]. The study [110] examined the change in the structure of the FeO_x coating on the LNMO surface annealed in a temperature range from 500 to 800 °C. It was found that as the annealing temperature increases, the stresses in the coating structure decrease (which should have a favorable effect on the electrochemical characteristics of the materials). However, annealing at higher temperatures can lead to the formation of a new undesirable phase. After annealing at 650 °C on the XRD patterns we observe changes in the intensity of some peaks, which is indirectly related to the location of heavy cations in the lithium nodes (8a) of the crystal lattice. For example, the ratio of intensities of peaks (311)/(400) is 1.02, 1.22, and 1.16 for the pure cathode, coated and annealed at 650 °C cathodes, and coated and annealed at 700 °C cathodes, respectively. The authors also attributed the presence of the peak (220) in the annealed samples to the occupation of lithium nodes by heavy transition metal cations. From the calculation of the energy of octahedral complexes according to the crystal field theory, the authors of the paper conclude that lithium sites are occupied by Fe^{3+} cations, which is also confirmed by the results of XAS studies (these cations presumably occupy the rib knots). At an annealing temperature of 700 °C, the α-Fe_2O_3 and Fe_3O_4 phases begin to appear, and iron cations begin to occupy octahedral LNMO voids (16d) that appear due to excessive doping of cathode structure. Therefore, the authors chose a temperature of 650 °C as an optimal temperature for iron oxide coating annealing (at this temperature, iron cations with a higher probability occupy tetrahedral voids). The EXAFS results confirm the choice of the optimal temperature: at 700 °C noticeable distortions in the oxygen anion sublattice are observed, which are less pronounced at 650 °C. It is also noted [110] that the films obtained by ALD method are deposited with defects in the crystal structure, which leads to cracks in the oxide film (SEM chipping). After annealing, these defects are not observed, indicating the cathode surface's restoration after annealing the FeOx structure. Additionally, the EDX studies found that after annealing, the iron ions penetrate to a greater depth of the cathode material.

Other coatings, such as HfO_2, are more stable, and metal (Hf) transition into the material bulk cannot be detected. For instance after annealing of HfO_2-coated NCM851005 material at 400 °C, no appreciable changes in the coating crystal structure (XRD), its morphology (SEM), and bonding energies (XPS) were detected [112]. The annealing resulted only in smoothing and compaction of the coating's surface (SEM of the chipping). Thus, the coating particles compacted and redistributed over the surface during the annealing process.

2.7. Characterization of the Near-Order Structure in Coatings and Their Relation to the Substrate

It is noted in most works that the positions of maxima on the XPS spectra of coatings (Al_2O_3—73.8 eV [42] < $Al2p_{3/2}$ < 75.8 eV [63], 531.2 eV [42] < O1s < 532.2 eV [55]; Ga_2O_3-$Ga3d_{5/2} \approx 21$ eV [98]; AlF_3—74.9 eV [103] < $Al2p_{3/2}$ < 75.2 eV [69], F1s = 685.2 eV [69]; CeO_2-$Ce3d_{3/2} \approx 901$ eV [104], $Ce3d_{5/2} \approx 898.6$ eV [104]; Fe_2O_3-$Fe2p_{3/2} = 711.5$ eV [107]; $FePO_4$-P2p = 133.3 eV [111]; MgO-Mg2p ≈ 49.5 eV [44]; ZnO-$Zn2p_{3/2} \approx 1021.5$ eV [130,131],

$2p_{1/2} \approx 1044.3$ eV [130,131]; ZrO_2-$Zr3d_{3/2}$ = 184.1 eV [133]) fall within the ranges of values characteristic of the respective substances. That is, the close environment of the elements in the coatings is the same as in the reference substances.

Several works [67,131,133] report differences in the position of maxima in the XPS spectra of modified particles and electrodes and attribute this to the different compositions and concentrations of functional groups. When studying the electrode coatings, they note that the position of the maxima corresponds to the values characteristic of these coatings. Shifts of the maxima toward lower binding energies are observed on the spectra of the coatings (ZnO-$Zn2p_{3/2} \approx 1019.35$ eV, $2p_{1/2}$ 1042.47 eV [131], ZrO_2 169.8 eV [132] < $Zr3d_{3/2}$ < 170.6 eV [133]) obtained during modification of cathode material powders [67,131–133]. In a study of lithium manganese spinel particles with applied coatings (Al_2O_3, ZnO, ZrO_2), chemical shifts were recorded both for the coating elements and for the $Mn2p_{1/2}$ and $Mn2p_{3/2}$ maxima characterizing the substrate [67]. According to the authors of the work, this phenomenon indicates the formation of chemical bonding between the cathode material particles and the coating's material (substrate-O-Me, Me: Al, Zr, Zn).

One study observed a change in film structure during synthesis: both $Zr3d_{3/2}$ (182 eV; 168 eV) maximums were observed on lithium manganese spinel particles modified by 50 cycles of sequential treatment with $Zr(OC(CH_3)_3)_4$ and H_2O vapors [134]. The micrographs (TEM) of the coating show two regions that differ in contrast. The darker one is located closer to the cathode material particle. The authors suggested that epitaxial growth occurs during the deposition process, and the region of the coating closer to the lithium-manganese spinel may have a long-range order. As the coating thickens, the influence of the substrate decreases, and the structure of the grown coating becomes amorphous. On the other hand, a study of amorphous ZrO_2 coatings grown on NCM(523) using $Zr(NMe_2)_4$ and H_2O vapors found a similar shift ≈ 13 eV of the $Zr3d_{3/2}$ maximum [132]. The shift is not caused by the crystallization of ZrO_2 coatings and finding its cause requires further investigation.

2.8. The Presence of a Crystalline Structure and the Density of Grown Coatings

When examining modified materials and electrodes using X-ray diffraction (XRD) analysis, the appearance of additional peaks caused by the deposited coatings is generally not observed. Considering that the particle diameter of the cathode material is a few micrometers, and the thickness of the coatings varies from units to tens of angstroms, the mass fraction of the grown coating phase in the studied material is below the sensitivity limit of XRD analysis. Taking this fact into account, thicker coatings of Al_2O_3 (≈ 50 nm, T = 120 °C) [46], $AlPO_4$ (50 cycles T = 250 °C) [101], ALPON (≈ 65 nm) [102], FeO_x (150 cycles, T = 450 °C) [109], NbO_x (30, 60 nm, T = 175 °C) [119], TiO_2 (100 cycles T = 120 °C) [123], ZrO_2 (100 cycles, T = 100 °C [45], 300 cycles T = 120 °C [133]) have been obtained and studied in a number of works.

In the works [43,44,83], the characteristic of the crystalline phase was not detected on the XRD patterns. In one of the considered works [133], a study of coatings using electron diffraction (SAED) revealed that its structure is polycrystalline. In this regard, we can conclude that the sensitivity of X-ray diffraction (XRD) analysis is insufficient to determine the crystalline state of even thicker (tens of nanometers) coatings. Only coatings grown of iron oxide on cathode material particles at 450 °C resulted in the appearance of peaks corresponding to the grown coating on XRD patterns [107]. This fact is related to the high synthesis temperature and to the deposition of the film not only on the external surface, but also due to the increase in the content of the modifying agent due to the introduction of the phase containing iron into the bulk of cathode material particles.

In almost all investigations where the cathode materials were examined, the TEM studies confirmed the presence of the crystalline phase [33,35,38,41,42,45,46,49,52,53,56, 64,65,67,68,98,111,112,118,123,131,134]. In contrast, regarding the TEM images of grown coatings of Al_2O_3 [33,35,38,41,42,45,46,49,52,53,56,64,65,67,75,80,88,90], Al_2O_3:Ga_2O_3 [98], AlF_3 [103], $AlPO_4$ [61,101], CeO_2 [49], $FePO_4$ [111], MgF_2 [118], Ta_2O_5 [120], TiO_2 [121–123], TiO_2-ZnO [125], TiO_2-Li_3PO_4 [126], ZnO [67,122], and ZrO_2 [49], the far order (crystal

structures) have not been found. The amorphous state of the coatings is related to their synthesis at low temperatures. Nevertheless, in the literature, experimental results testify the possibility of the application on cathode powder particles, coatings with a crystalline structure—ZnO [68,133], ZrO_2 [68], as well as coatings including both crystalline and amorphous phases—ZrO_2 [134]. As a possible reason for the presence of a crystalline phase, it is suggested that the film structure aligns with the crystalline structure of the cathode material (substrate) due to epitaxial growth [134]. Epitaxial growth is also observed in [109].

The density of the coating can be estimated based on the value of growth per synthesis cycle (growth rate). Calculations have shown that the density of the grown coatings (Al_2O_3—3.6 g/cm^3 [44], MgO—2.9 g/cm^3 [44], MgF_2—2.4–2.7 g/cm^3 [118], ZrO_2—5.6 g/cm^3 [44]) is lower than the values typical of the bulk phases of the corresponding substances. The lower value of the coating density is caused by the relatively large size of the precursors [44]. Therefore, achieving a denser concentration per surface unit of chemically sorbed molecules is impossible.

2.9. Evaluation of Coating Growth Rate and Influencing Factors

Since cathode materials are disperse and electrodes are porous, it is difficult to determine the thickness of thin coatings. Therefore, the average growth per cycle is estimated based on the average growth per cycle obtained by synthesizing coatings of the same composition on model objects (e.g., silicon wafers). A more accurate method is to determine thicknesses based on the increments per cycle calculated from transmission microscopy data for the same modification objects but with a significantly higher number of cycles.

The possible increase in the coating thickness per cycle on dispersed cathode materials and electrodes as compared to flat substrates seems to be caused by side processes of film deposition from the gas phase [39]. Gas-phase deposition can occur due to incomplete removal of reagents. For example, in the case of aluminum oxide synthesis, high growth rates may not have a significant effect on the film structure [65]. Whereas, in the case of titanium dioxide grown, side reactions can lead to the formation of coatings consisting of small particles. Increasing the blowing time of the reaction space from 5 to 20 s significantly reduced the number of formed particles [45], which indicates the incomplete removal of reagents during the desorption stage.

2.10. Choice between Modifying Active Material Particles or Finished Electrodes

Since the ALD method allows for the coating of powder and electrode particles, the question of comparing the characteristics of modified electrodes and electrodes obtained from modified cathode materials is logical.

As a result of studies [70], it was found that the aluminum oxide layer on the particle surface can be damaged in the process of electrode preparation. Aluminum oxide has low electronic conductivity. Therefore, electrodes prepared from modified particles will have lower electronic conductivity than uncoated electrodes, and consequently, there will be a more intense reduction in the charge-discharge capacity. When the electrode is coated, the film growth occurs not only on the cathode material but also on the conductive additive and binder. The decrease in the intensities and shift toward lower binding energies of the peaks related to the binder (PVDF) may be due to partial doping of the binder in the film-grown process [29]. Keeping the cathode material particles in contact with the network of conductive particles of the electrically conductive additive allows the charge to be effectively dissipated [46].

3. Effects of Coatings on the Functional Properties of Modified Cathode Materials and Electrodes

This section will discuss:
- the primary studies' results of changes in the coating structure that take place during cycling;
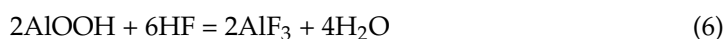
- physicochemical effects leading to improvement of functional properties of cathode materials or positive electrodes;
- the list of observed effects on the electrochemical properties of cathode materials or positive electrodes;
- effect of coatings of different compositions on electronic, ionic conductivity, lithium diffusion resistance through thin films, charge transfer resistance, performance at high potentials, and a large number of charge-discharge cycles, etc.

3.1. Physical and Chemical Processes in Coatings during Lithium Intercalation/Deintercalation during Charge-Discharge of Modified Cathode Materials and Electrodes

Many articles [73,74,83,90,97,100,112,114,117,120,122–124,135,136] have noted that coating the cathode material to a greater extent affects the capacity preservation of the cathode material, and the greater the coating thickness, the longer the capacity is preserved during cycling. The observed increase in cycling life is related to the fact that the coating markedly reduces side reactions with the cathode material [91,93,116,124] (in particular, dissolution of transition metals [95,100,114,123,139,140] with their subsequent deposition as SEI films on the anode [93]).

In the study [74], an XPS investigation of the cathodes after cycling were conducted, which showed that the coated and uncoated cathode materials have C=O peaks after cycling, and the uncoated cathode has higher carbon-oxygen bonding energy, which is explained by increased Li_2CO_3 compound formation. Additionally, for the uncoated cathode material, the standard $LiPF_xO_y$ peak characterizing the electrolyte decomposition reaction on the cathode surface is observed. On the other hand, only LiF and AlF_3 peaks are observed for the coated material, which suggests that during cell cycling, the main electrolyte reactions took place with the coating and affected the cathode core to a lesser extent.

Another reason for preserving the capacitance is to increase the stability of the secondary particles of the cathode material. In the work of [117], the presence of cracks on the cathode after cycling was investigated using SEM. It was shown that the uncoated cathode material exhibited significantly more cracks, which were also more extensive. Such crack formation also affects the geometric characteristics of the cathode material. During cycling, its "swelling" was observed. The SEM images of the coated cathode material after cycling at an elevated temperature of 50 °C [90] show that the coating homogeneity decreases during cycling, and the formation of holes of regular geometry down to the active cathode material is observed. As a possible explanation, the authors suggested that hydrofluoric acid is formed during cycling, which can react with Al_2O_3 and AlOOH. During these reactions, a large amount of water is released, which reacts with the electrolyte to synthesize hydrofluoric acid, i.e., an autocatalytic reaction occurs.

$$Al_2O_3 + 6HF = 2AlF_3 + 3H_2O \tag{5}$$

$$2AlOOH + 6HF = 2AlF_3 + 4H_2O \tag{6}$$

$$LiPF_6 + H_2O = LiF + POF_3 + 2HF \tag{7}$$

The processes occurring during the modification of cathode materials with aluminum oxide and titanium oxide coatings are the most studied (see Figure 1b and references to these coatings in Tables 1–5). In this regard, as their example, let us consider the methods and results of studies of the processes occurring in the coatings during the charge-discharge of cathode materials.

When studying lithiation processes of aluminum oxide nanofilm, it was found [81,141], that Li-Al-O glass is formed in the film and a similar phase can form on the surface of aluminum oxide coated cathode materials during charge-discharge. On the other hand, considering the insignificant shift (0.2 eV) of the $Al2p_{3/2}$ maximum into a lower energy range after 10 charge-discharge cycles of $Li_{1.2}Ni_{0.13}Mn_{0.54}Co_{0.13}O_2$ cathode material covered with aluminum oxide, the authors of study [65] concluded that no Li-Al-O glass formation was caused by lithium passing through the aluminum oxide film. In similar studies of titanium

dioxide coatings in the XPS spectra of the sample, after the charge-discharge, the maxima related to the titanium ions Ti^{3+} and Ti^{4+} were detected. Therefore, the presence of Ti^{3+} ions in the film was attributed to the lithiation reaction of titanium oxide [65].

On the differential capacity curve (dQ/dV) of modified aluminum oxide there is only one peak characterizing the cobalt reduction process [31]. In this regard, the authors conclude that Al^{3+} is not involved in the electrochemical process. Similar studies of TiO_2-coated $LiCoO_2$ in the 3.8 V region found maxima on the differential charge-discharge curves. Their presence seems to be due to the formation of the $LiTi_yCo_{1-y}O_{2+0.5y}$ phase at the $LiCoO_2/TiO_2$ boundary [31]. Partial doping with titanium atoms is also associated with this process and the increased capacity of the modified lithiated cobalt oxide.

Thus, aluminum oxide is not an electrochemically active material during the charge-discharge of modified cathode materials and electrodes. The question of the formation of Li-Al-O glass in the process of lithium passage is still open. A study of titanium oxide coatings found that this type of coating can participate in the electrochemical reaction and increase the discharge capacity of the cathode material.

During the study of LCO cathode degradation at high charge voltages, it was found [139], that the destruction of this cathode material is directly due to two factors:

- the formation of a large concentration of unstable Co^{4+} cation, which goes into the electrolyte;
- the reorganization of the cathode structure from hexagonal to monocline (due to cobalt dissolution).

In this case, the protective coating on the cathode's surface plays a buffer role: Co^{4+} ions, instead of dissolving in the liquid electrolyte, begin to form a solid electrolyte phase in the coating, which in turn favorably affects the cyclic life of the battery.

3.2. CV Studies before and after Coating

The chemical composition and structure of the coating affect the reactions in the coating and cathode material. Two strong peaks are observed in the CV study of the uncoated NMC sample in [78]. The first peak at 4.2 V characterizes the change in the oxidation degree of Ni^{2+}-Ni^{4+} and Co^{3+}-Co^{4+}, the second peak at 4.6 V appears due to the activation of the Li_2MnO_3 phase. No new peaks were observed during the cycling of the sample coated with aluminum oxide, which testifies to the absence of coating material contribution to the measured capacity during charging-discharging of the cathode material. However, the intensity of the peak responsible for the Li_2MnO_3 phase formation (4.6 V) is markedly lower, which allows us to assume that coating Al_2O_3 can reduce the electrolyte oxidation on the cathode and increase its Coulomb efficiency. The analysis of the first derivatives of the differential capacity curve (dQ/dV) of such a system was performed in paper [74]. It was found that during the film growth, there was no significant shift in the peaks' characteristics of bare NMC (two peaks were observed on all curves: phase transitions in hexagonal and monoclinic syngonies during lithiation/delamination processes). However, the intensity of the peaks decreased significantly, indicating that the phase transition between hexagonal and monoclinic syngonies (which, according to the authors [74], is caused by the Jahn-Teller effect for transition metal ions) was irreversible. It is not fully known which mechanism is responsible for the interaction of the coating with the cathode materials. However, experiments show that the dissolution of transition metals in the electrolyte is significantly reduced due to coating, and the passivation of parasitic reactions is observed.

Studies of FeO_x and annealed FeO_x coatings on the Li-rich (LMR) cathode [109] showed a slight difference in the Coulomb efficiency after the first charge-discharge cycle. Thus, for the annealed FeO_x sample, the Coulomb efficiency was 80.3%, for the coated FeO_x sample, it was 79.3%, and for the uncoated sample, it was 76.3%, which indicates a greater degree of Li and O atom conservation in the lattice of the coated cathode material during its activation. Additionally, for the iron oxide-coated samples, a decrease in the intensity of the peak at 2.8 V is observed, which is associated with the presence of Li ions in the spinel structure.

When comparing the CV curves of bare LNMO and LNMO coated with $AlPO_4$ film [101], neither additional peaks nor a significant shift of the original peaks was observed. However, the intensity of the original peaks (near 4.7 V, which is responsible for the Ni^{2+}/Ni^{3+} and Ni^{3+}/Ni^{4+} redox reaction) is markedly lower for the coated sample. The combination of the data suggests that the coating is electrochemically inactive during cyclic charge-discharge, and Li ions uniformly pass through the $AlPO_4$ coating.

3.3. Resistance of the Coating during Cycling

The stability of aluminum oxide films on the electrode surface during electrochemical cycling can be evaluated by analyzing the shape and intensity of the $Al2p_{3/2}$ band of XPS spectra. The band intensity can decrease without a significant change in shape [31]. Thus, dissolution of the aluminum oxide coating occurs, and its fluorination products cannot be detected. Furthermore, the signal intensity from titanium atoms after charge-discharge of titanium oxide coated cathode materials under comparable conditions decreases for a smaller number of cycles. Thus, the titanium dioxide film is less stable compared to the aluminum oxide film.

Some works report the observation of gradual fluorination of the aluminum oxide film. For example, in the paper [56], after 300 cycles of charge-discharge, the $Al_{2p3/2}$ maximum was observed to shift toward higher bonding energies and to be broadened. Assuming that the observed shift of the maximum position is associated with the replacement of oxygen atoms by fluorine in the environment, the authors decomposed the band into two components. With the increase in the number of ALD cycles from 10 to 50, the share of the curve area characterizing the presence of Al-F bonds became smaller. Consequently, the fraction of aluminum atoms bonded to fluorine atoms decreases in thicker coatings. The presence of maxima related to Al-O and Al-F may indicate an incomplete course of the Reaction (8).

$$Al_2O_3 + 6HF => 2AlF_3 + H_2O \qquad (8)$$

Thermodynamic calculations evidenced the possible joint presence of Al-O and Al-F bonds in the aluminum oxide film exposed to HF [142]. In the case of the interaction of ZnO with HF, according to thermodynamic calculations [142], the formation of the end products of the reaction—ZnF_2 and H_2O is preferable. In this regard, the aluminum oxide film is more stable when exposed to HF.

Thus, of the considered oxide coatings (Al_2O_3, TiO_2, ZnO), the Al_2O_3 film is the most resistant to dissolution upon interaction with HF. However, since the products of partial fluorination are observed, and in some cases are not observed in the study of coatings during cycling, the reaction mechanism probably depends on the conditions of the experiment.

In work [87], when the NMC cathode was coated with AlF_3 film after battery cell cycling, an additional peak of 685.75 eV was detected in the F1s region, which is located between two components: LiF and Al_2O_3 by energy. This peak presumably characterizes the presence of the $LiAlF_4$ compound. Additionally, no peak indicating PDVF decomposition on the cathode material was detected for these cells, i.e., during cell cycling, the Al_2O_3 film is lithified by AlF and LiF components. The phase turns out to $LiAlF_4$ is more stable in the electrolyte environ, which as a result, affects the cycling stability since there is no excessive electrolyte decomposition [87].

3.4. Physical and Chemical Effects Leading to Improved Functional Properties of Cathodes

The modification of cathode materials affects their surface's physical and chemical properties. The change is primarily because the coatings' and cathode material's chemical nature differ. In some cases, the growth process can affect the structure and hence the material layers' properties close to the cathode materials' outer surface. For example, in studies [102,127] the effect of doping $AlPO_4$ and $TiPO_4$ films with nitrogen was studied; the authors showed that due to doping of the films at high charge-discharge currents, a reduced

energy barrier for redox reactions is observed, which favorably affects the cycling life of layouts at high currents.

3.4.1. Reducing the Intensity of Metal Dissolution

Electrodes including NCM(111) modified with $LiTaO_3$ coating after charge-discharge in the potential range 3.0–4.7 V were kept in LIB electrolyte at 60 °C for 14 days. According to the chemical analysis data, the concentration of Ni, Co, and Mn in the electrolyte during the modified electrode exposure was significantly lower than during the exposure of the bare electrode. Thus, the coatings can partially prevent the dissolution of cathode materials when interacting with hydrofluoric acid in the form of traces present in the electrolyte. The need to reduce the dissolution of the cathode material is related not only to the loss of the active component but also to the reduction in the transition metal content of the cathode material in the SEI film on the surface of the anode material. For example, it was shown in [48] that the coating of the anode material can affect the battery life due to a decrease in the content of nickel and manganese in the SEI film. In addition, the deposition of transition metals on the separator and anode reduces the cycling life due to an increase in the battery's internal resistance [35].

Additionally, a decrease in transition metals solubility is noted in the paper [83], where the HE-NCM cathode coating with an Al_2O_3 film was investigated. The ICP-AES study of the electrolyte revealed that the dissolution of transition metals of uncoated material is 4 times more intense than that of ALD-coated material.

On the contrary, in the article [73], the authors note the presence of an increase in the dissolution of Mn during LMO coating with Al_2O_3 film. Such results are attributed to the reaction of an aluminum oxide film with hydrofluoric acid, resulting in the formation of the AlF3 compound is water, which again interacts with the electrolyte salt to form a new HF, which subsequently dissolves Mn ions, i.e., there is a flow of autocatalysis.

In article [100], bare LNMO and LNMO coated with AlF_3 film were kept in the electrolyte for one and two weeks at 45 °C. In both cases, the amount of dissolved manganese in the electrolyte is always higher than the nickel (for all samples). The deposited coating allows protection of the cathode even after two weeks of exposure to the electrolyte (the concentration of manganese, in this case, is three times lower than in the case of the experiment with the uncoated sample). The study [123] compared XPS spectra before and after cell cycling. Before cycling, the XPS showed peaks at 642.1, and 643.7 eV, corresponding to the presence of Mn^{3+} and Mn^{4+} in the structure, with the Mn^{3+} fraction for the LMO titanium oxide coated cathode being 57.8% and 58.2% for the uncoated one. After the cycling, the Mn^{4+} fraction increased from 41.8% to 42.8%, which suggests the formation of the λ-MnO_2 phase during the charge-discharge process. This assumption is confirmed by the presence of a 1 eV shift of the manganese peak to the lower energies (towards an increasing degree of manganese oxidation). For the titanium oxide coated sample, only a slight increase in the Mn^{4+} fraction (by 0.2%) and, consequently, less degradation of the cathode material was observed. At the same time, changes in the titanium peaks were observed for the coated sample: after cycling, their positions were 459.7 and 465.4 eV (compared to the initial 458.9 and 464.6 eV), which is explained by the presence of a Ti-O and Ti-F transition bond, i.e., Ti-O-F. During the ToF-SIMS study, the TiO_xF_y, phase was detected on the surface of the titanium oxide coating; the aggregate of the results obtained allows us to assert that the coating reacted with hydrofluoric acid and water in a higher priority than the cathode material.

A study [95] examined the effect of Al_2O_3 and CeO_2 coatings of the LMO cathode on the dissolution of Mn from the cathode structure. The ICP-AES was used to obtain transition metal dissolution data by measuring the manganese ratios in the electrolyte solution after two and four weeks of holding at room temperature and 55 °C. Each coating composition was synthesized on the cathode. The coatings were 1.5 and 3 nm thick. It was found that regardless of the presence and type of coating, the dissolution of manganese from the cathode structure increased with increasing temperature. Additionally, it was

observed that in the presence of the CeO_2 film, Mn dissolution was more intense than for the bare cathode and the cathode coated with Al_2O_3 film. As the thickness of the Al_2O_3 coating increased, the dissolution of Mn decreased.

In contrast, the opposite effect was observed for the CeO_2 films [95], i.e., as the thickness increased, the transition metal dissolution also increased. The vacancy formation energy of Mn in the cathode structure was calculated for the uncoated cathode, cathode coated with Al_2O_3, and cathode coated with CeO_2, it was: 8.91, 11.71, and 6.49 eV, respectively. These vacancy formation energies indicate that depending on the coating applied, the Mn-O bond length changes, which entails a decrease or increase in the degree of removal of Mn from the cathode structure. Additionally, the authors of the article [95] mention studies of manganese dissolution from LMO when it is coated with MgO Cr_2O_3, Co_3O_4, TiO_2, ZnO, and ZrO_2, films. For each coating, the vacancy formation energy is 5.91, 8.89, 7.09, 9.02, 9.16, and 9.02 eV, respectively. Consequently, the application of TiO_2, ZnO, and ZrO_2 films prevents the dissolution of Mn to a greater extent compared to the bare cathode.

3.4.2. Decrease in the Growth Rate of the Solid-Electrolyte Film during the Charge-Discharge Process

To determine the effect of protective coatings on the CEI film structure, the original $LiNi_{0.5}Mn_{1.5}O_4$ and the material modified with four ALD cycles were studied using surface-sensitive methods [41,54]. When studying samples of cathode materials after 50 charge-discharge cycles at 30 °C using XPS, it was found that the modified cathode material has [41]:

1. higher intensity of the C-C peak (285 eV), which characterizes the presence of PVDF and carbon black;
2. higher intensity of the O1s, which peak characterizing the Ni(II)O bond (530.3 eV);
3. lower intensity of maxima characterizing organic compounds (alkyl carbonates), Li_2CO_3, and LiPFxOy;
4. higher intensity of the maximum characterizing the bond of the fluorine atom (685.6 eV) with lithium or aluminum.

The results obtained allowed the authors [41] to conclude that the CEI film of the modified cathode material contained fewer organic molecules. The smaller increase in the thickness of the organic component of the film was also confirmed by secondary ion mass spectrometry with time-of-flight mass separation (TOF-SIMS). Therefore, reducing the CEI film thickness leads to a minor increase in resistance at the cathode during LIB operation. In addition, a thinner CEI film indicates less electrolyte decomposition during LIB work [29].

3.4.3. Suppression of Undesirable Processes (Changes in the Degree of Oxidation of Metal Ions and Phase Transitions) in the Layers of Cathode Materials Located near the Outer Surface of Cathodes

In the study [57], the X-ray absorption near fine structure (XANES) during charge-discharge of the original and aluminum oxide modified $LiNi_{0.4}Mn_{0.4}Co_{0.2}O_2$ was investigated. It was shown that:

5. the coating suppresses the oxidation of Co^{3+} to Co^{4+}, causing the release of active oxygen;
6. charge compensation during lithium removal ($Li_{(1-x)}Ni_{0.4}$-$Mn_{0.4}Co_{0.2}O_2$, where $0 \leq x \leq 0.5$) is due to nickel oxidation.

The authors attribute the shown reversible oxidation of nickel to the fact that the aluminum oxide film prevents interaction between the electrolyte and active oxygen nucleophilic atoms bound to nickel.

The initial sample $Li_{1.2}Ni_{0.2}Mn_{0.6}O_2$ and the one modified with aluminum oxide (4 cycles) were studied using electron energy loss spectroscopy (EELS) after 40 charge-discharge cycles [64]. Based on the chemical shift of the L_3 band, the valence states of manganese on the surface and in the layers close to the surface of the cathode material were determined. It was found that in the uncoated sample, Mn^{2+} ions were present near

the outer surface of the particle. However, as one moves deeper into the particle, there is a relatively thick layer in which Mn^{3+} ions are present. In contrast, the study of the modified material revealed that only near the surface of the cathode material is the partial reduction in manganese detectable, with an average oxidation degree greater than +3. Thus, the aluminum oxide coating suppresses the reduction in manganese at the cathode/electrolyte interface, slowing the transition of manganese to the electrolyte.

The charge of the cathode material NCM(523) to the potential of 4.5 V led to the fact that the reflections from the cobalt and manganese atoms almost completely disappeared in the XPS spectra [55]. The position of the maximum in the nickel spectrum indicated that the nickel was in the degree of oxidation +2. After argon ion surface etching of the charged cathode material, the shape of the Ni, Co, and Mn spectra approached that of the spectra of the uncharged cathode material. Aluminum oxide coating (5 cycles) prevented the noted changes in the XPS spectra. Examination of the uncoated sample by transmission electron microscopy showed that after 100 charge-discharge cycles in the range of 3.0–4.5 V, the NiO phase was present in the near-surface layer of the cathode material. Thus, the interaction of the electrolyte with the cathode material leads to a partial reduction in nickel atoms and the formation of the NiO phase, which slows down the movement of lithium ions and increases the resistance. The cathode material modified with aluminum oxide retained the initial phase composition.

Aluminum oxide coating also prevents the phase transition of the layered structure into a spinel structure occurring on the surface of cathode materials as the number of charge-discharge cycles increases [7,64,71].

In work [93], it was found that during cycling, changes on the surface of NMC(811) occur, namely, oxygen vacancies are formed; simultaneously, an increase in the intensity of the XPS peaks for nickel is observed. After cycling, all transition metal peaks are shifted to lower bonding energies, indicating that the degree of oxidation of transition metals during cyclic charge-discharge decreases. The authors also note that the cathode surface is enriched with Mn atoms after cyclic tests. The phenomena described above were not observed for cathodes coated with Al_2O_3 film.

3.4.4. Study of the Resistance of Films

Researchers use impedance spectroscopy to study changes in film resistance. Impedance spectra before formation are usually quite challenging to interpret. In this regard, studies after at least one cycle of charge and discharge are considered in the works. The measurement is carried out at full charge or at a given potential after some time (up to 10 h [57]), which is necessary to establish the equilibrium of the processes taking place.

Interpretation of the resulting spectra can be conducted as a descriptive analysis of the semicircles [29,35,36,39,71,82,84,86,88,91,108,112,126,127,139], or with calculation of resistance components based on the selected equivalent electronic circuit [45,49,53,72,75–77,87,89,101,109,110,113–115,117,119–122,124,125,135,136].

When interpreting the impedance spectra presented in the Nyquist coordinates—(Z''–Z') several areas located in different frequency ranges are distinguished. A minimum at high frequencies (100 kHz) characterize the ohmic component of the impedance of the electrode, and it includes the contribution from the electronic conductivity of the electrode, the ionic conductivity of the electrode, as well as the electronic resistance of contacts (cell current leads, current collectors). Next, two (three) half-circles, whose maximums are located at approximately 10 kHz or 1 kHz, are observed (or, by mathematical processing, are identified). Based on the shape of the curve at the high-frequency spectrum region (maximum at $\approx$10 kHz) it is possible to determine the resistance to the movement of ions through a thin solid electrolyte film (R_f) and the electronic resistance (R_b) between active material particles (which is rarely mentioned [29,51]). The charge transfer resistance (R_{CT}) can be determined based on a mathematical treatment of the half-circle shape with a maximum at $\approx$1 kHz. At lower frequencies (<1 kHz), a straight line with about 45° slope characterizing the process of lithium diffusion into the bulk of cathode material

particles is observed. Based on this linear dependence, the diffusion coefficient can be calculated [53,76,77,114,125,130,132].

Taking into account the possible physical and chemical processes, an equivalent electrical circuit is selected (several equivalent circuits were found in the reviewed literature—1 [7,45,49,53,55,61,74,77,84,87–89,104,107–110,113,121,122,124,125,130,132,135,136], 2 [33,41, 56,72,111,114,119], 3 [118], 4 [115], 5 [51], 6 [57], 7 [82,113], 8 [86,114], 9 [75,120], 10 [75], 11 [117], 12 [117] see Appendix A Table A2) and by selecting the parameters of a chosen circuit (capacitance, inductance, resistance), a minimum discrepancy with the impedance spectrum is achieved. Then, the resistances R_f, R_b, R_{CT} and their changes as a result of coating application can be determined (effect of thickness [7,29,33,55,56,61,74,84,86, 89,104,107,111,114,115,119,132,133] and nature of coating [7,45,49,84,89–91,109,110,112,113, 117,122,124,125,136,139], coating on electrode [87,101,114,119,120,122,124,125,135] or particles [72,74–77,82,84,86,88–91,108–110,112,113,117,126,133,136]). Additionally, the changes in resistances can be noticed in other electrochemical tests (cyclic charge-discharge at room and elevated temperature [76,104,107], charge-discharge potential range [53,74,76], exposure time at high potentials [42,90]).

It is reasonable to determine the effect of coating on ionic conductivity without charging the cathode to high potentials (above the stability of the electrolyte boundary) because the lower lithium ionic conductivity through the SEI film may be due to the presence of a denser SEI film on the surface of unmodified samples. Thus, uncoated samples may have higher resistivity when charged to high potentials due to film formation from electrolyte decomposition products.

The electronic conductivity of the grown films is usually lower than of the cathode materials, in this regard the conductivity of the cathode materials with the coatings can be reduced. Doped AlF with W or mixed Al_2O_3/Ga_2O_3 coatings can be used as a possible technique to reduce the conductivity.

Based on the reviewed literature, the following generalizations can be made:

1. coating the cathode material particles or the electrode generally does not increase Rf and RCT resistances. Rf and RCT resistances. Exceptions are studies [74,75,87,110,117, 122,124,125], but in most cases the modified ones have lower resistances after cycling;
2. an optimum in coating thickness is observed;
3. in the process of testing, the resistances tend to increase. For the modified ones, the increase is less noticeable;
4. the exposure time, at high potentials, leads to the intensive growth of the solid-electrolyte film, coating grown slows down this process.

3.4.5. Electronic and Ionic Conductivity

Coating primarily affects the surface properties of the modified cathode materials. As a rule, the electronic conductivity of the grown coatings is lower than that of the cathode materials. Therefore, one can observe a decrease in electronic conductivity due to the modification.

The electronic conductivity of some cathode materials are as follows: LCO is 10^{-4} Sm/cm [39], NCM is 10^{-5} Sm/cm [143], LMO is 10^{-6} Sm/cm [144], LMR is 5×10^{-7} Sm/cm [145], LNMO is 10^{-5} Sm/cm [146]. The uncoated cathode materials have higher electronic conductivity than materials with coatings (for example Al_2O_3 is 10^{-14} Sm/cm [39], CeO_2 is 2.5×10^{-8} Sm/cm [147], TiO_2 is 10^{-11} Sm/cm [148] ZnO is 7.2×10^{-7} Sm/cm [149] ZrO_2 is 10^{-10} Sm/cm [150]). Modified LCO powder particles as a result of 2–10 cycles of $AlCH_3$ and H_2O vapor treatment at 120 °C led to an order of magnitude decrease in electronic conductivity to 10^{-5} Sm/cm. An increase in the electronic conductivity of grown coatings can be achieved by introducing more conductive components, for example, Ga_2O_3 (Al_2O_3:Ga_2O_3) [98] or W/WC_x (AlW_xF_y) [103,151].

The discharge curves presented at different discharge currents (GCD) show that the coating of TiO_2-Li_3PO_4 on the LNMO cathode probably significantly increases the electronic

and ionic conductivity, as compared to the uncoated electrode, there is a smaller decrease in capacitance with increasing discharge current (in the 0.1C to 5C range) [126].

In the study [74], in the range of 3.0–4.5 V, a pair of peaks responsible for the phase transition between the hexagonal and monoclinic crystal structures are observed on the differential capacity analysis (dQ/dV) curves of the uncoated cathode. In addition to these clear peaks on the curves at high voltages in the region of oxidative reactions, we also observe weaker peaks of monoclinic to a hexagonal structure phase transition, which shift to lower voltages with an increasing number of charge-discharge cycles and become less intensive. For the coated cathode, similar peaks are observed, but with lower intensity and a small voltage shift. During the cycling of the uncoated cathode, a decline in the intensity of peaks is observed, which is caused by the irreversibility of the phase transition, which the authors of the paper associate with the Jahn-Teller effect [74].

The article [109] describes the investigation of FeO_x coating the electronic conductivity. The cold-pressed pellets were used for the study. The results showed an increase in conductivity by half an order of magnitude (40 cycles ALD FeOx compared to bare cathode) with an increasing number of ALD cycles. When the number of ALD cycles increases from 40 to 100, a decline in conductivity is observed (i.e., the dependence of conductivity on the number of ALD cycles has a maximum), and such results are associated with iron oxidation to degree 3+ (at layering 100 cycles), which is characterized by reduced electronic conductivity. The observed decrease in the discharge capacity of the cathode material is also associated with a decrease in electronic conductivity.

The decrease in electronic conductivity after coating LCO material with niobium oxide was also observed in the article [119]. The authors have made this conclusion on the base of cyclic voltammetry curves. The decrement of the peaks' intensity responsible for lithium intercalation and deintercalation (3.9 V) and the transition from the hexagonal to monocline phase (4.0 and 4.2 V) was associated with an increase in electronic resistance.

The effect of the number of treatment cycles on the conductivity of the modified cathode material ($LCO + Al_2O_3$) was shown in [39]. After coating application during 2–10 treatment cycles, the electronic conductivity decreased by an order of magnitude. In the case of electrode modification, there should be no intense decrease in the electronic conductivity because the particles of the cathode material retain contact with the particles' network of the conductive additive, at least for thin layers of coatings (1–6 cycles).

The application of thin coatings also influences ionic conductivity. For example, in an EIS study [119], the authors note an increase in the Li diffusion coefficient (10^{-7} Sm/cm) in the coating layer (Niobium oxide on LCO). In [124], the increase in lithium-ion diffusion is also noted. When TiO2 coating was applied to NCM(523), the uncoated cathode had ionic conductivity in full cells of 0.083 Sm/cm, while the coated cathodes with coatings obtained at different temperatures had ionic conductivity of: 0.090 (120 °C), 0.091 (150 °C) and 0.120 (180 °C) Sm/cm.

A study of the effect of CeO_2 coating on the diffusion coefficient and electronic conductivity of LMO at different coating thicknesses was described in [105]. The authors note that when the coating thickness is less than 3 nm, the diffusion coefficient augments with increasing coating thickness; when the coating thickness is greater than 3 nm, the diffusion coefficient decreases with a further increase in thickness. Furthermore, the authors note that when considering diffusions in bulk and on the surface in thin coatings, diffusion on the surface plays a significant role, and the presence of an extremum point in the diffusion coefficient on coating thickness dependence can be explained by the formation of diffusion channels between the electrode and the coating.

The diffusion coefficient was measured for electrodes made of modified particles. In most cases, the modification did not lead to a decrease in the diffusion coefficient, and in some cases even increased it. The formation of compounds with increased lithium conductivity Li-Al-O, $Li-Al_2O_3$ and Li-Zr-O was suggested as an explanation for the increase in diffusion, and a movement mechanism inside the modifier coating was proposed [59].

3.4.6. Effect of Film Annealing on the Electrochemical Characteristics of Batteries

After annealing coated materials, a number of articles have noted the following: a smaller decrease in capacity during cycling [91,108–110,112,136], increased capacity at high discharge currents [108–110,112,136], decreased resistance growth during cycling charge-discharge [136], increased Li diffusion coefficient [108,109].

3.5. Summary List of Observed Effects on the Electrochemical Properties of Cathode Materials or Positive Electrodes during Coating

As a result of ALD coating of cathode materials and positive electrodes, the following effects on their performance were observed:

- the cathode capacity decreases less during cycling [7,29,30,32,34,35,43,45,50,51,64,66,67, 72,75–78,80,82,83,85–89,91,93,95,97,100,101,103,107–110,112–114,116,117,119–128,130,132, 134–136,139,140,152];
- increases cycling life and capacity when charged to high potentials [7,33,42,48,53,55, 63,80,82,99,107,108,111,123,125,132,139];
- Coulomb efficiency increases [33,41,82,85,103,112,113,120];
- self-discharge is reduced [41,123];
- overvoltage on the cathode material can be reduced [35,44];
- increased ability to work at elevated temperatures [35,48,67,71,95,100,107,121,124,132–134];
- increases the capacity when discharging with high currents [33,56,72,74–78,84,89,91, 92,94,99–103,107–114,116,119–121,123–128,132,133,135,136];
- thermal stability in the charged state increases [53,101,116,122];
- polarization increases [37,38,51,55,115,152];
- polarization decreases [100,101,111,122];
- there is no effect of lithium-rich cathode materials on voltage reduction during cyclic charge-discharge [30,66];
- the growth of resistance during cycling is reduced [7,33,42,53,56,107,111,119,121–123, 136,153].

4. Comparison of Coatings of Different Compositions

A number of publications have attempted to compare the efficiency of coatings of different compositions. When comparing the results, curves of change in the capacity as a function of the number of cycles or the discharge current are used. The comparison is made relative to the cathode materials coated with an aluminum oxide film. Summarizing the results of the above studies (Tables 6 and 7), it can be concluded that in all cases considered $LiAlO_2$ ($LiAlO_x$) film, as well as CeO_2 coating, provided the best cycling life and serviceability of electrodes at high discharge currents as compared to Al_2O_3 film. Experimental results are described in the literature, according to which cathode materials coated with ZrO_2, ZnO, and TiO_2 had worse and better performance than cathode materials coated with Al_2O_3. The advantage of the Al_2O_3 film is attributed to its greater resistance to HF. The better performance of cathode materials modified with ZrO_2, ZnO, and TiO_2 is explained by their higher conductivity than Al_2O_3 film.

Table 6. Effect of coating selection on the capacity of active cathode materials in charge-discharge with different currents.

Material	P/E	Current, C	C_p	Reference
$LiCoO_2$	P	0.1	$4ZnO > 4Al_2O_3$	[39]
$LiCoO_2$	E	$\approx 0.6 \div \approx 4$	$2ZrO_2 \approx 2TiO_2 > 2Al_2O_3$	[45]
$LiCoO_2$	E	$1 \div 2$	$15 \text{ nm}NbO_x > 30 \text{ nm}NbO_x$ $> 60 \text{ nm}NbO_x$	[119]
	E	$5 \div 100$	$15 \text{ nm}NbO_x \approx 30 \text{ nm}NbO_x$ $> 60 \text{ nm}NbO_x$	

Table 6. *Cont.*

Material	P/E	Current, C	C_p	Reference
LiCoO$_2$	–	0.25	LiMeO > LiMeP > MeF~MeP	[139]
LiMn$_2$O$_4$	P	0.2 ÷ 1 (25 °C)	50CeO$_2$ < 5ZrO$_2$ < 5Al$_2$O$_3$	[49]
	P	2 (25 °C)	50CeO$_2$ > 5Al$_2$O$_3$ > 5ZrO$_2$	
	P	0.2 ÷ 2 (55 °C)	50CeO$_2$ > 5ZrO$_2$ > 5Al$_2$O$_3$	
LiMn$_2$O$_4$	E(P)	1 ÷ 200	5 nmTiO$_2$ > 1 nmAl$_2$O$_3$	[47]
LiMn$_2$O$_4$	E	0.2 ÷ 0.5 (25 °C)	10TiO$_2$ ≈15TiO$_2$ > 40TiO$_2$	[123]
	E	0.2 (55 °C)	10TiO$_2$ ≈ 15TiO$_2$ > 40TiO$_2$	
	E	0.5 (55 °C)	15TiO$_2$ > 10TiO$_2$ > 40TiO$_2$	
(523)	P	0.1 ÷ 10	MgO ≈ ZrO$_2$ > Al$_2$O$_3$	[44]
(523)	P	1/3	2Al$_2$O$_3$ > 8Al$_2$O$_3$	[80]
(523)	E	0.2 ÷ 5	5Ta$_2$O$_5$ > 2Ta$_2$O$_5$ > 10Ta$_2$O$_5$	[120]
(523)	E	0.1	100TiO$_2$ (synthesis at 180 °C) ≈ 100TiO$_2$ (synthesis at 120 °C) > 100TiO$_2$(synthesis at 150 °C)	[124]
		0.2 ÷ 1	100TiO$_2$(synthesis at 180 °C) ≈ 100TiO$_2$(synthesis at 150 °C) ≈ 100TiO$_2$(synthesis at 120 °C)	
		2	100TiO$_2$(synthesis at 180 °C) > 100TiO$_2$(synthesis at 150 °C) > 100TiO$_2$(synthesis at 120 °C)	
(622)	P	1 ÷ 3	4Al$_2$O$_3$ ≈ 10Al$_2$O$_3$	[85]
(622)	E	0.1 ÷ 0.5; 3	20ZrO$_2$ ≈ 5ZrO$_2$ ≈ 40ZrO$_2$	[135]
	E	1 ÷ 2	20ZrO$_2$ > 5ZrO$_2$ > 40ZrO$_2$	
(622)	P	0.1 ÷ 2	20Al$_2$O$_3$ > 10Al$_2$O$_3$ ≈ 40Al$_2$O$_3$	[74]
(622)	E	0.1 ÷ 5	10Li$_x$Ti$_y$O$_z$ > 50TiO$_x$	[117]
(622)	P	0.1 ÷ 0.2 (25 °C)	2ZrO$_2$ ≈ 5ZrO$_2$ ≈ 8ZrO$_2$	[136]
	P	0.5 ÷ 5 (25 °C)	2ZrO$_2$ > 5ZrO$_2$ > 8ZrO$_2$	
(622)	P	0.1 ÷ 0.5	1AlPON ≈ 2AlPO$_4$	[102]
	P	1 ÷ 5	1AlPON > 2AlPO$_4$	
(811)	P	0.1 ÷ 2 (25 °C)	2Al$_2$O$_3$ ≈ 5Al$_2$O$_3$ > 10Al$_2$O$_3$	[86]
	P	0.1 ÷ 5 (50 °C)	2Al$_2$O$_3$ > 5Al$_2$O$_3$ ≈ 10Al$_2$O$_3$	
FCG (811)	P	0.1 ÷ 5	Al$_2$O$_3$ > TiO$_2$	[7]
NCA	P	0.5 ÷ 2	TiO$_2$ > Al$_2$O$_3$	
LiNi$_{0.5}$Mn$_{1.5}$O$_4$	E	0.1 ÷ 0.33	5LiAlO$_2$ > 5Al$_2$O$_3$	[48]
LiNi$_{0.5}$Mn$_{1.5}$O$_4$	P	≈0.1 ÷ 2	Al$_2$O$_3$ > TiO$_2$	[33]
LiNi$_{0.5}$Mn$_{1.5}$O$_4$	P	0.1 ÷ 5	10(TiO$_2$-LiPO$_4$)> LiPO$_4$ ≈ TiO$_2$	[126]
LiNi$_{0.5}$Mn$_{1.5}$O$_4$	P	0.1	5Al$_2$O$_3$ > 10Al$_2$O$_3$ > 20Al$_2$O$_3$	[90]
L1	P	0.1	6ZnO ≥ 6ZrO$_2$ > 6Al$_2$O$_3$	[68]
	P	0.2 ÷ 5	6ZrO$_2$ > 6ZnO > 6Al$_2$O$_3$	
L4	E	0.04 ÷ 1	4ZnO-6TiO$_2$ > 6TiO$_2$-4ZnO≈ ≈3TiO$_2$-4ZnO-3TiO$_2$	[125]
L4	E	0.04 ÷ 1	10TiO$_2$ > 5ZnO	[122]
L7	P	–	24Al$_2$O$_3$ ≈ 40Al$_2$O$_3$ > 16Al$_2$O$_3$	[82]

Table 6. *Cont.*

Material	P/E	Current, C	C_p	Reference
LiFePO$_4$	P	0.1 ÷ 5 (25 °C)	5TiN > 5 Al$_2$O$_3$ > 10TiN	[89]
	P	10 (25 °C)	5TiN > 10TiN > 5 Al$_2$O$_3$	
LiFePO$_4$	P	1 ÷ 5 (25 °C)	10TiN > 15TiN ≈ 2Al$_2$O$_3$ ≈ 5TiN > 5Al$_2$O$_3$ > >10Al$_2$O$_3$	[84]
	P	10 ÷ 15 (25 °C)	10TiN > 15TiN > 5TiN ≈ 5Al$_2$O$_3$ > 2Al$_2$O$_3$> >10Al$_2$O$_3$	
	P	1 ÷ 5 (55 °C)	10TiN > 15TiN ≈ 2Al$_2$O$_3$ ≈ 5TiN > 5Al$_2$O$_3$ > >10Al$_2$O$_3$	
	P	10 ÷ 15 (55 °C)	10TiN > 15TiN > 5TiN ≈ 5Al$_2$O$_3$ > 2Al$_2$O$_3$ > >10Al$_2$O$_3$	

Footer. C_p—capacitances values comparison (more or less) of cathode materials modified with different coatings (the number before the formula is the number of ALD cycles); FCG—see note to Table 3; E(P)—thin-film electrode.

Table 7. Effect of coating selection on capacity retention of active cathode materials during cyclic charge-discharge.

Material	P/E	Discharge Current, C	Comparison of Capacities at the End of Cycling Tests	Reference
LiCoO$_2$	P	0.1	4Al$_2$O$_3$ > 4ZnO	[39]
LiCoO$_2$	E	≈1	2Al$_2$O$_3$ > ZrO$_2$ ≈ 2TiO$_2$	[45]
LiCoO$_2$	E	0.2	10Al$_2$O$_3$ > 50TiO$_2$	[31]
LiCoO$_2$	E	1	2AlF$_3$ > 2Al$_2$O$_3$	[69]
LiCoO$_2$	E	10	30 nmNbO$_x$ > 60 nmNbO$_x$ > 15 nmNbO$_x$	[119]
LiCoO$_2$	–	0.5 (3–4.6 V)	LiMeP > MeF > MeP > LiMeO	[139]
		0.5 (3–4.55 V)	MeF > LiMeP > Me > LiMeO	
LiMn$_2$O$_4$	P	1(25 °C)	6ZnO > 6ZrO$_2$ > 6Al$_2$O$_3$	[67]
	E	1(25 °C)	6ZnO > 6ZrO$_2$ > 6Al$_2$O$_3$	
	P	1(55 °C)	6ZnO > 6ZrO$_2$ > 6Al$_2$O$_3$	
	E	1(55 °C)	6ZrO$_2$ > 6ZnO > 6Al$_2$O$_3$	
LiMn$_2$O$_4$	P	1(25 °C)	50CeO$_2$ > 5Al$_2$O$_3$ ≥ 5ZrO$_2$	[49]
	P	1(55 °C)	50CeO$_2$ > 5ZrO$_2$ > 5Al$_2$O$_3$	
	P	2(25 °C)	50CeO$_2$ > 5Al$_2$O$_3$ > 5ZrO$_2$	
LiMn$_2$O$_4$	P	–	5Al$_2$O$_3$ > 10Al$_2$O$_3$	[73]
LiMn$_2$O$_4$	E	0.5(25 °C)	10TiO$_2$ ≈ 15TiO$_2$ > 40TiO$_2$	[123]
	E	0.5(55 °C)	15TiO$_2$ > 10TiO$_2$ > 40TiO$_2$	
LiMn$_2$O$_4$	P	(25 °C)	100CeO$_2$ > 5Al$_2$O$_3$	[95]
LiMn$_2$O$_4$	P	(55 °C)	5Al$_2$O$_3$ > 100CeO$_2$	[95]
(523)	P	1	Al$_2$O$_3$ > MgO ≈ ZrO$_2$	[44]
(523)	P	–	2Al$_2$O$_3$ > 8 Al$_2$O$_3$	[80]
(523)	E	1	5Ta$_2$O$_5$ > 2Ta$_2$O$_5$ > 10Ta$_2$O$_5$	[120]

Table 7. *Cont.*

Material	P/E	Discharge Current, C	Comparison of Capacities at the End of Cycling Tests	Reference
(523)	E	1(55 °C)	$100TiO_2$ (synthesis at 180 °C) > $100TiO_2$ (synthesis at 150 °C) > $100TiO_2$ (synthesis at 120 °C)	[124]
(622)	P	1	$4Al_2O_3 \approx 10Al_2O_3$	[85]
(622)	E	0.5	$20ZrO_2 > 5ZrO_2 > 40ZrO_2$	[135]
(622)	P	0.5	$20Al_2O_3 > 10Al_2O_3 > 40Al_2O_3$	[74]
(622)	E	1	$10Li_xTi_yO_z > 50TiO_x$	[117]
(622)	P	1 (25 °C); 1 (50 °C)	$TiPO_4 > TiPON$	[127]
(622)	P	1 (25 °C)	$5ZrO_2 > 2ZrO_2 > 8ZrO_2$	[136]
(622)	P	1	$1AlPON > 2AlPO_4$	[102]
(811)	P	1 (25 °C)	$2Al_2O_3 \approx 5Al_2O_3 > 10Al_2O_3$	[86]
	P	5 (50 °C)	$2Al_2O_3 > 5Al_2O_3 \approx 10Al_2O_3$	
(811)	P	0.1	$20Al_2O_3 > 10Al_2O_3 > 50Al_2O_3$	[88]
FCG (811)	P	0.3; 1	$Al_2O_3 > TiO_2$	[7]
NCA	P	0.3; 1	$TiO_2 > Al_2O_3$	
$LiNi_{0.5}Mn_{1.5}O_4$	E	0.1; 0.33	$5LiAlO_2 > 5Al_2O_3$	[48]
$LiNi_{0.5}Mn_{1.5}O_4$	P	0.5	$10(TiO_2\text{-}LiPO_4) > LiPO_4 \approx TiO_2$	[126]
$LiNi_{0.5}Mn_{1.5}O_4$	P	0.5 (25 °C)	$5Al_2O_3 > 10Al_2O_3 > 20Al_2O_3$	[90]
	P	0.5 (50 °C)	$20Al_2O_3 > 5Al_2O_3$	
$LiNi_{0.5}Mn_{1.5}O_4$	P	0.1	$2AlF_3$ (synthesis at 240 °C) > $2AlF_3$ (synthesis at 150 °C) > $4AlF_3$ (synthesis at 150 °C)	[100]
$LiNi_{0.5}Mn_{1.5}O_4$	E	1	$50Li_3PO_4 > 83Li_3PO_4 > 17Li_3PO_4$	[114]
L1	P	1	$6ZrO_2 > 6ZnO > 6Al_2O_3$	[68]
L2	E	<0.1	$6LiAlO_x > 6ZrO_2 > 6TiO_2 > 5Al_2O_3$	[30]
L4	E	1	$4ZnO\text{-}6TiO_2 > 3TiO_2\text{-}4ZnO\text{-}3TiO_2 > 6TiO_2\text{-}4ZnO$	[125]
L4	E	0.5	$10TiO_2 > 5ZnO$	[122]
L7	P	–	$24Al_2O_3 > 40Al_2O_3 \approx 16Al_2O_3$	[82]
L10	–	1 (25 °C)	$10LiTaO_3 > 5LiTaO_3 > 2LiTaO_3 \approx 20LiTaO_3$	[116]
NMC	E	1 (25 °C)	$1AlF_3\text{-}5Al_2O_3 > 2AlF_3\text{-}4Al_2O_3 > 6Al_2O_3 \approx 6AlF_3 \approx 4AlF_3\text{-}2Al_2O_3 \approx 5AlF_3\text{-}1Al_2O_3$	[87]
$LiFePO_4$	P	2 (25 °C)	$5TiN > 5Al_2O_3 > 10TiN$	[89]
	P	5 (25 °C)	$5TiN > 10TiN > 5Al_2O_3$	

Comparisons of the effects of ALD coatings with other methods of improving the performance of cathode materials are very rare. In particular, it was found in [29] that the aluminum oxide coated electrode with the ALD retained its capacity better during cycling and had lower resistance than the electrode containing aluminum oxide particles. The authors attribute the observed effect to the fact that the films obtained by the ALD method are more tightly bound to the cathode material than the aluminum oxide particles introduced during electrode fabrication.

The choice of the optimum coatings thickness of different compositions is conditioned by the fact that for cathode operation, it is a requirement to find a compromise between protective properties and conductivity (electrical and ionic) of the coating. Therefore, achieving optimal electrochemical characteristics is mainly ensured after up to ten synthesis cycles of modifying coatings (see Tables 1–5).

5. Conclusions

The presented work demonstrated analysis of the current literature on the application of atomic layer deposition in improving the final characteristics of lithium-ion batteries through the modification of cathode materials. More than one hundred articles devoted to this topic were analyzed.

This paper presents the basic principles of the atomic layer deposition, its advantages (conformality of coatings, ability to obtain coatings on the developed geometry, low synthesis temperatures, etc.), and disadvantages (in particular, those related to the subsequent investigation of the obtained coatings).

The analysis revealed that the most popular cathodes for modification are: lithiated cobalt oxide (LCO), lithiated manganese spinel (LMO), lithiated nickel-cobalt-manganese oxides (NCM), lithiated nickel-manganese spinel (LNMO), various non-stoichiometric compositions from those presented above with excess lithium (LMR); the most popular modification materials are: aluminum oxide (Al_2O_3), titanium oxide (TiO_2), and zirconium oxide (ZrO_2). Furthermore, the influence of cathode surface modification on the physico-chemical processes occurring during the charging-discharging of layouts was considered.

During the conducted research on the influence of coating deposition on output characteristics of cathodes, it has been revealed that, in most cases, the dependence of output capacity on the thickness of applied coating passes through the maximum. Thus, we can conclude that at modification of cathodes for lithium-ion energy, it is necessary to find a compromise between the grown thickness of coating and batteries' output characteristics, so for the most studied coatings, optimum thickness is about 1 nm (Al_2O_3, TiO_2, ZrO_2).

The positive influence of coatings on such practical parameters of batteries as cyclic life, capacity life during discharging by increased currents, self-discharge, thermal stability, performance at increased temperatures, etc. can be deduced from the analyzed publications.

Author Contributions: Conceptualization, Y.K.; data curation, Y.K., D.O. and A.R.; investigation, Y.K., D.O. and A.R.; project administration, M.M.; supervision, M.M.; writing—original draft preparation, Y.K. and D.O.; writing—review and editing, Y.K. and M.M. All authors have read and agreed to the published version of the manuscript.

Conflicts of Interest: The authors declare no conflict of interest.

Abbreviations

The following abbreviations are used in this manuscript:

ALD	atomic layer deposition
GCD	galvanostatic charge-discharge
CAM	cathode active material
Cap. ret.	capacity retention
CCS	chemical current source
CVD	chemical vapor deposition
CV	cyclic voltammetry

dQ/dV	differential capacity analysis
DSC	differential scanning calorimetry
EIS	electrochemical impedance spectroscopy
EELS	electron energy loss spectroscopy
EDS	X-ray energy dispersive spectroscopy
ICP-AES	inductively coupled plasma atomic emission spectroscopy
GITT	galvanostatic intermittent titration technique
LCO	cathode material with stoichiometry similar with $LiCoO_2$
LIB	lithium-ion battery
LMO	cathode material with stoichiometry similar with $LiMn_2O_4$
LNMO	cathode material with stoichiometry similar with $LiNi_{0.5}Mn_{1.5}O_4$
LMR	lithium- and manganese-rich cathode material with a layer structure
MLD	molecular layer deposition
NCA(XYZ)	cathode material with $LiNi_{0.8<x<0.92}Co_{0.03<y<0.15}Al_{0.02<z<0.05}O_2$ structure
NCM(XYZ)	cathode material with $LiNi_{x/(x+y+z)}Co_{y/(x+y+z)}Mn_{z/(x+y+z)}O_2$ structure
Raman	Raman spectroscopy
Rate cap.	rate capability
SEM	scanning electron microscopy
SIMS	secondary-ion mass spectrometry
SAED	selected area electron diffraction
TG	thermogravimetric analysis
TEM	transmission electron microscopy
XAFS	X-ray absorption fine structure
XANES	X-ray absorption near edge structure
XAS	X-ray absorption spectroscopy
XRD	X-ray diffraction
XPS	X-ray photoelectron spectroscopy

Appendix A

Table A1. List of the main studies in the field of cathode modification by the ALD method.

Coatings	EELS	EDS	DSC, TG	ICP-AES	Raman	SAED	SEM	SIMS	TEM	XANES	XAS	XPS	XRD	Cap. ret.	CV	dQ/dV	EIS	GCD	GITT	Rate cap.	Reference
		X					X					X		X			X				[29]
														X			X				[30]
									X							X					[31]
					X		X		X					X		X					[32]
		X		X			X					X	X				X			X	[33]
		X	X				X					X		X		X					[34]
		X					X					X	X				X				[35]
	X					X	X					X	X				X			X	[36]
												X	X				X				[37]
Al$_2$O$_3$						X	X		X								X				[38]
												X	X				X				[39]
													X				X				[40]
		X										X	X				X				[70]
												X	X				X				[25]
					X		X		X			X	X				X			X	[71]
				X								X	X				X				[41]
							X		X			X	X				X				[42]
												X	X				X				[43]
							X					X	X							X	[44]

Table A1. *Cont.*

Coatings	EELS	EDS	DSC, TG	ICP-AES	Raman	SAED	SEM	SIMS	TEM	XANES	XAS	XPS	XRD	Cap. ret.	CV	dQ/dV	EIS	GCD	GITT	Rate cap.	Reference
		■		■			■		■					■				■		■	[45]
							■		■			■		■						■	[46]
							■							■	■			■		■	[47]
		■				■	■		■					■				■		■	[7]
											■		■				■			■	[48]
									■				■				■			■	[49]
													■								[50]
		■			■		■						■					■		■	[51]
		■					■					■				■				■	[52]
		■	■				■					■		■		■		■			[53]
		■					■					■	■			■		■			[54]
					■						■	■							■		[55]
		■	■		■		■						■				■			■	[56]
									■	■			■	■							[57]
		■					■		■					■			■				[58]
												■	■		■		■				[59]
							■						■	■							[60]
		■			■		■		■		■	■	■								[61]
							■					■	■				■			■	[62]
												■	■	■			■				[63]
■		■					■		■			■	■	■							[64]
							■						■	■			■				[65]
				■									■	■							[66]
							■		■				■		■						[67]
							■					■	■	■						■	[68]
							■					■	■	■							[69]
									■				■	■				■		■	[72]
													■	■				■			[73]
		■					■						■	■				■			[74]
				■			■		■			■	■	■				■			[75]
													■	■			■	■			[76]
				■					■					■	■			■			[77]
									■				■				■				[78]
		■			■				■			■	■								[79]
		■					■		■				■							■	[80]
		■		■			■					■	■					■		■	[81]
				■			■					■	■				■			■	[82]
				■								■		■						■	[83]
												■	■				■				[84]
		■		■			■		■			■	■	■						■	[85]
												■	■	■				■			[86]
												■	■	■							[87]
		■			■		■		■			■	■	■				■			[88]
		■	■				■					■	■	■				■			[89]
■				■					■			■	■								[90]
				■									■	■			■				[91]
												■	■					■			[92]
■				■								■	■	■							[93]
		■					■					■	■	■						■	[94]
				■					■				■	■							[95]
												■		■							[96]
		■					■						■	■			■	■		■	[97]
Al₂O₃-AlF₃																	■				[87]
Al₂O₃-Ga₂O₃		■							■			■	■							■	[98]

Table A1. *Cont.*

Coatings	EELS	EDS	DSC, TG	ICP-AES	Raman	SAED	SEM	SIMS	TEM	XANES	XAS	XPS	XRD	Cap. ret.	CV	dQ/dV	EIS	GCD	GITT	Rate cap.	Reference
AlF$_3$							■		■			■								■	[99]
							■					■	■	■			■				[69]
AlF$_3$		■		■			■		■			■	■	■				■		■	[87]
		■		■			■		■			■	■	■		■	■				[100]
AlPO$_4$		■		■			■		■			■	■	■			■				[61]
		■		■			■		■			■	■	■		■	■				[101]
		■					■					■	■	■			■				[102]
AlPON		■					■					■	■	■			■				[102]
AlW$_x$F$_y$						■			■			■	■			■		■			[103]
									■			■		■						■	[49]
		■					■		■			■		■				■			[104]
CeO$_2$				■			■					■	■	■							[105]
				■								■									[106]
				■					■					■	■						[95]
Fe$_2$O$_3$		■	■	■		■	■		■			■	■	■			■	■			[107]
	■	■	■	■		■	■		■			■	■	■			■				[108]
FeO$_x$	■	■		■		■	■		■			■	■	■			■	■			[109]
		■		■			■					■	■	■			■				[110]
FePO$_4$		■			■		■		■			■	■			■					[111]
HfO$_2$		■		■					■			■		■							[112]
LiAlO$_2$												■		■						■	[48]
LiAlO$_x$														■							[30]
LiF		■		■			■					■	■	■							[113]
Li$_3$PO$_4$		■					■		■			■	■	■			■				[113]
		■							■			■	■	■							[114]
LiTaO$_3$		■		■					■			■	■	■			■				[115]
		■		■								■	■	■							[116]
Li$_x$Ti$_y$O$_z$		■										■		■						■	[117]
Me$_x$O$_y$												■		■						■	[139]
MeF$_x$												■		■						■	[139]
MgF$_2$		■					■		■			■		■			■				[118]
MgO							■					■		■			■			■	[44]
NbO$_x$							■	■						■			■			■	[119]
Ta$_2$O$_5$									■			■		■			■			■	[120]
TiO$_2$														■						■	[30]
												■		■		■				■	[31]
		■		■			■				■	■	■							■	[33]
												■	■	■			■			■	[45]
												■		■						■	[47]
		■				■	■		■			■		■						■	[7]
TiO$_2$		■					■					■	■	■			■				[121]
									■			■	■	■			■			■	[65]
		■	■				■		■			■	■	■						■	[122]
		■		■			■					■	■	■		■				■	[123]
												■	■	■			■				[124]
TiO$_2$-ZnO		■					■		■			■	■	■			■				[125]
TiO$_2$-Li$_3$PO$_4$		■					■		■			■	■	■			■				[126]
TiO$_x$		■					■					■	■	■			■				[117]
TiN														■			■			■	[84]
		■		■			■					■		■						■	[89]
TiPO$_4$														■			■			■	[127]
TiPON														■			■			■	[127]

Table A1. *Cont.*

Coatings	EELS	EDS	DSC, TG	ICP-AES	Raman	SAED	SEM	SIMS	TEM	XANES	XAS	XPS	XRD	Cap. ret.	CV	dQ/dV	EIS	GCD	GITT	Rate cap.	Reference
V$_x$O$_y$							■		■											■	[128]
		■					■		■				■		■			■			[129]
												■	■	■			■				[39]
ZnO							■		■			■	■	■	■		■	■		■	[130]
		■					■		■			■	■	■	■						[131]
							■		■			■	■	■							[67]
							■		■			■		■						■	[68]
		■					■					■		■		■	■			■	[122]
												■		■							[30]
					■				■			■	■							■	[132]
ZrO$_2$							■					■		■				■			[44]
		■		■					■	■		■						■			[45]
									■			■	■	■			■				[49]
		■				■						■		■							[133]
		■					■					■		■							[134]
									■			■	■			■					[67]
												■		■						■	[68]
		■										■		■			■	■		■	[135]
		■		■			■		■			■		■						■	[136]

Table A2. Selectable equivalent circuits in impedance spectroscopy studies.

Circuit Number	Equivalent Circuit
1	Rs — (CPE1 ∥ Rf) — (CPE2 ∥ Rct) — Wo1
2	R1 — (CPEf ∥ Rf) — (CPEdl ∥ Rct) — Wo1
3	R1 — (CPE1 ∥ [R2 — (CPE2 ∥ [R3 — Wo1])])
4	Re — (Rsl ∥ Csl) — (Rct ∥ Cdl) — Wo1
5	Rs ol — (Csf ∥ Rsf) — (Cb ∥ Rb) — (Cdl ∥ Rct) — Zw
6	Rs — (Rint ∥ CPEint) — (Rct ∥ CPEct) — Zw — CPEdl
7	Rs — (CPE1 ∥ Rct) — Wo1
8	Rs — (CPE1 ∥ Rct)
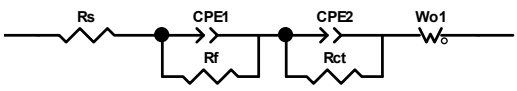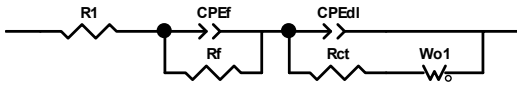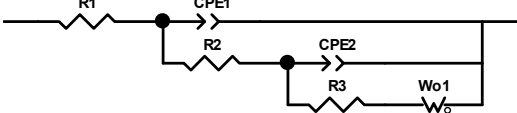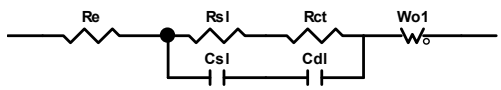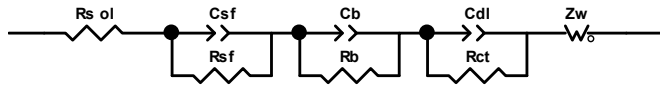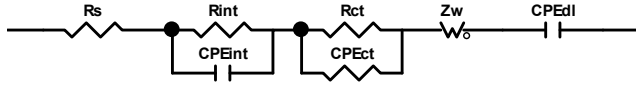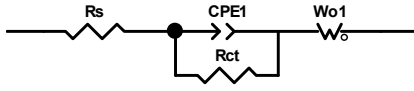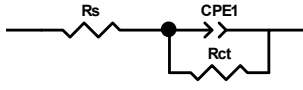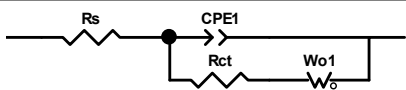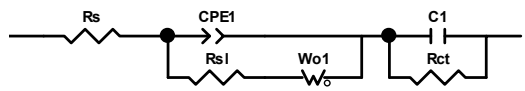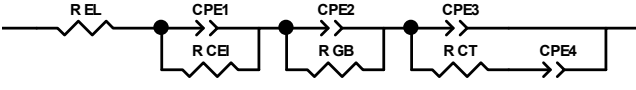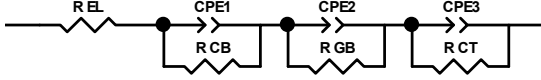
Table A2. *Cont.*

Circuit Number	Equivalent Circuit
9	
10	
11	
12	

References

1. Lu (Mark), H.-L. Commercial Technology & Product Development Trends of Cathode & Anode Materials for LIB in 2015. In Proceedings of the Second International Forum on Cathode & Anode Materials for Advanced Batteries, Xiaoshan, Hang Zhou, China, 22 April 2015; p. 55.
2. Dislich, H.; Hinz, P. History and principles of the sol-gel process, and some new multicomponent oxide coatings. *J. Non-Cryst. Solids* **1982**, *48*, 11–16. [CrossRef]
3. Vahlas, C.; Caussat, B.; Serp, P.; Angelopoulos, G.N. Principles and applications of CVD powder technology. *Mater. Sci. Eng. R Rep.* **2006**, *53*, 1–72. [CrossRef]
4. Malygin, A.A.; Drozd, V.E.; Malkov, A.A.; Smirnov, V.M. From V. B. Aleskovskii's "Framework" Hypothesis to the Method of Molecular Layering/Atomic Layer Deposition. *Chem. Vap. Depos.* **2015**, *21*, 216–240. [CrossRef]
5. Puurunen, R.L. A Short History of Atomic Layer Deposition: Tuomo Suntola's Atomic Layer Epitaxy. *Chem. Vap. Depos.* **2014**, *20*, 332–344. [CrossRef]
6. Puurunen, R.L. Surface chemistry of atomic layer deposition: A case study for the trimethylaluminum/water process. *J. Appl. Phys.* **2005**, *97*, 52. [CrossRef]
7. Mohanty, D.; Dahlberg, K.; King, D.M.; David, L.A.; Sefat, A.S.; Wood, D.L.; Daniel, C.; Dhar, S.; Mahajan, V.; Lee, M.; et al. Modification of Ni-Rich FCG NMC and NCA Cathodes by Atomic Layer Deposition: Preventing Surface Phase Transitions for High-Voltage Lithium-Ion Batteries. *Sci. Rep.* **2016**, *6*, 16. [CrossRef]
8. Poodt, P.; Cameron, D.C.; Dickey, E.; George, S.M.; Kuznetsov, V.; Parsons, G.N.; Roozeboom, F.; Sundaram, G.; Vermeer, A. Spatial atomic layer deposition: A route towards further industrialization of atomic layer deposition. *J. Vac. Sci. Technol. A* **2012**, *30*, 11. [CrossRef]
9. Donders, M.E.; Knoops, H.C.M.; Kessels, W.M.M.; Notten, P.H.L. Remote Plasma Atomic Layer Deposition of Thin Films of Electrochemically Active LiCoO₂. *ECS Trans.* **2011**, *41*, 321–330. [CrossRef]
10. Donders, M.E.; Arnoldbik, W.M.; Knoops, H.C.M.; Kessels, W.M.M.; Notten, P.H.L. Atomic Layer Deposition of LiCoO₂ Thin-Film Electrodes for All-Solid-State Li-Ion Micro-Batteries. *J. Electrochem. Soc.* **2013**, *160*, A3066–A3071. [CrossRef]
11. Miikkulainen, V.; Ruud, A.; Ostreng, E.; Nilsen, O.; Laitinen, M.; Sajavaara, T.; Fjellvag, H. Atomic Layer Deposition of Spinel Lithium Manganese Oxide by Film-Body-Controlled Lithium Incorporation for Thin-Film Lithium-Ion Batteries. *J. Phys. Chem. C* **2014**, *118*, 1258–1268. [CrossRef]
12. Liu, J.; Banis, M.N.; Sun, Q.; Lushington, A.; Li, R.Y.; Sham, T.K.; Sun, X.L. Rational Design of Atomic-Layer-Deposited LiFePO4 as a High-Performance Cathode for Lithium-Ion Batteries. *Adv. Mater.* **2014**, *26*, 6472–6477. [CrossRef]
13. Popovich, A.A.; Maximov, M.Y.; Novikov, P.A.; Silin, A.O.; Nazarov, D.V.; Rumyantsev, A.M. Cyclic stability of the anode material based on tin(IV) oxide for thin-film current sources. *Russ. J. Appl. Chem.* **2016**, *89*, 679–681. [CrossRef]
14. Nazarov, D.V.; Maximov, M.Y.; Novikov, P.A.; Popovich, A.A.; Silin, A.O.; Smirnov, V.M.; Bobrysheva, N.P.; Osmolovskaya, O.M.; Osmolovsky, M.G.; Rumyantsev, A.M. Atomic layer deposition of tin oxide using tetraethyltin to produce high-capacity Li-ion batteries. *J. Vac. Sci. Technol. A* **2017**, *35*, 11. [CrossRef]
15. Ahmed, B.; Anjum, D.H.; Gogotsi, Y.; Alshareef, H.N. Atomic layer deposition of SnO2 on MXene for Li-ion battery anodes. *Nano Energy* **2017**, *34*, 249–256. [CrossRef]
16. Kazyak, E.; Chen, K.H.; Wood, K.N.; Davis, A.L.; Thompson, T.; Bielinski, A.R.; Sanchez, A.J.; Wang, X.; Wane, C.M.; Sakamoto, J.; et al. Atomic Layer Deposition of the Solid Electrolyte Garnet Li₇La₃Zr₂O₁₂. *Chem. Mater.* **2017**, *29*, 3785–3792. [CrossRef]
17. Hamalainen, J.; Holopainen, J.; Munnik, F.; Hatanpaa, T.; Heikkila, M.; Ritala, M.; Leskela, M. Lithium Phosphate Thin Films Grown by Atomic Layer Deposition. *J. Electrochem. Soc.* **2012**, *159*, A259–A263. [CrossRef]

18. Nilsen, O.; Miikkulainen, V.; Gandrud, K.B.; Ostreng, E.; Ruud, A.; Fjellvag, H. Atomic layer deposition of functional films for Li-ion microbatteries. *Phys. Status Solidi A-Appl. Mater. Sci.* **2014**, *211*, 357–367. [CrossRef]

19. Knoops, H.C.M.; Donders, M.E.; van de Sanden, M.C.M.; Notten, P.H.L.; Kessels, W.M.M. Atomic layer deposition for nanostructured Li-ion batteries. *J. Vac. Sci. Technol. A* **2012**, *30*, 10. [CrossRef]

20. Jung, Y.S.; Cavanagh, A.S.; Gedvilas, L.; Widjonarko, N.E.; Scott, I.D.; Lee, S.H.; Kim, G.H.; George, S.M.; Dillon, A.C. Improved Functionality of Lithium-Ion Batteries Enabled by Atomic Layer Deposition on the Porous Microstructure of Polymer Separators and Coating Electrodes. *Adv. Energy Mater.* **2012**, *2*, 1022–1027. [CrossRef]

21. Chen, H.; Lin, Q.; Xu, Q.; Yang, Y.; Shao, Z.P.; Wang, Y. Plasma activation and atomic layer deposition of TiO_2 on polypropylene membranes for improved performances of lithium-ion batteries. *J. Membr. Sci.* **2014**, *458*, 217–224. [CrossRef]

22. Snyder, M.Q.; Trebukhova, S.A.; Ravdel, B.; Wheeler, M.C.; DiCarlo, J.; Tripp, C.P.; DeSisto, W.J. Synthesis and characterization of atomic layer deposited titanium nitride thin films on lithium titanate spinel powder as a lithium-ion battery anode. *J. Power Sources* **2007**, *165*, 379–385. [CrossRef]

23. Wang, H.Y.; Wang, F.M. Electrochemical investigation of an artificial solid electrolyte interface for improving the cycle-ability of lithium ion batteries using an atomic layer deposition on a graphite electrode. *J. Power Sources* **2013**, *233*, 1–5. [CrossRef]

24. Wang, D.N.; Yang, J.L.; Liu, J.; Li, X.F.; Li, R.Y.; Cai, M.; Sham, T.K.; Sun, X.L. Atomic layer deposited coatings to significantly stabilize anodes for Li ion batteries: Effects of coating thickness and the size of anode particles. *J. Mater. Chem. A* **2014**, *2*, 2306–2312. [CrossRef]

25. Jung, Y.S.; Lu, P.; Cavanagh, A.S.; Ban, C.; Kim, G.H.; Lee, S.H.; George, S.M.; Harris, S.J.; Dillon, A.C. Unexpected Improved Performance of ALD Coated $LiCoO_2$/Graphite Li-Ion Batteries. *Adv. Energy Mater.* **2013**, *3*, 213–219. [CrossRef]

26. Meng, X.B.; Yang, X.Q.; Sun, X.L. Emerging Applications of Atomic Layer Deposition for Lithium-Ion Battery Studies. *Adv. Mater.* **2012**, *24*, 3589–3615. [CrossRef]

27. Liu, J.; Sun, X.L. Elegant design of electrode and electrode/electrolyte interface in lithium-ion batteries by atomic layer deposition. *Nanotechnology* **2015**, *26*, 14. [CrossRef]

28. Ahmed, B.; Xia, C.; Alshareef, H.N. Electrode surface engineering by atomic layer deposition: A promising pathway toward better energy storage. *Nano Today* **2016**, *11*, 250–271. [CrossRef]

29. Bettge, M.; Li, Y.; Sankaran, B.; Rago, N.D.; Spila, T.; Haasch, R.T.; Petrov, I.; Abraham, D.P. Improving high-capacity $Li_{1.2}Ni_{0.15}Mn_{0.55}Co_{0.1}O_2$-based lithium-ion cells by modifiying the positive electrode with alumina. *J. Power Sources* **2013**, *233*, 346–357. [CrossRef]

30. Bloom, I.; Trahey, L.; Abouimrane, A.; Belharouak, I.; Zhang, X.F.; Wu, Q.L.; Lu, W.Q.; Abraham, D.P.; Bettge, M.; Elam, J.W.; et al. Effect of interface modifications on voltage fade in $0.5Li_{(2)}MnO_{(3)}$center dot $0.5LiNi_{(0.375)}Mn_{(0.375)}CO_{(0.25)}O_{(2)}$ cathode materials. *J. Power Sources* **2014**, *249*, 509–514. [CrossRef]

31. Cheng, H.M.; Wang, F.M.; Chu, J.P.; Santhanam, R.; Rick, J.; Lo, S.C. Enhanced Cycleabity in Lithium Ion Batteries: Resulting from Atomic Layer Depostion of Al_2O_3 or TiO_2 on $LiCoO_2$ Electrodes. *J. Phys. Chem. C* **2012**, *116*, 7629–7637. [CrossRef]

32. Cheng, Q.; Yang, T.; Li, Y.; Li, M.; Chan, C.K. Oxidation-reduction assisted exfoliation of $LiCoO_2$ into nanosheets and reassembly into functional Li-ion battery cathodes. *J. Mater. Chem. A* **2016**, *4*, 6902–6910. [CrossRef]

33. Cho, H.M.; Chen, M.V.; MacRae, A.C.; Meng, Y.S. Effect of Surface Modification on Nano-Structured $LiNi_{0.5}Mn_{1.5}O_4$ Spinel Materials. *Acs Appl. Mater. Interfaces* **2015**, *7*, 16231–16239. [CrossRef]

34. Choi, M.; Ham, G.; Jin, B.S.; Lee, S.M.; Lee, Y.M.; Wang, G.X.; Kim, H.S. Ultra-thin Al_2O_3 coating on the acid-treated $0.3Li_{(2)}MnO_{(3)}$center dot $0.7LiMn_{(0.60)}Ni_{(0.25)}Co_{(0.15)}O_{(2)}$ electrode for Li-ion batteries. *J. Alloy. Compd.* **2014**, *608*, 110–117. [CrossRef]

35. Fang, X.; Ge, M.Y.; Rong, J.P.; Che, Y.C.; Aroonyadet, N.; Wang, X.L.; Liu, Y.H.; Zhang, A.Y.; Zhou, C.W. Ultrathin Surface Modification by Atomic Layer Deposition on High Voltage Cathode $LiNi_{0.5}Mn_{1.5}O_4$ for Lithium Ion Batteries. *Energy Technol.* **2014**, *2*, 159–165. [CrossRef]

36. Fang, X.; Lin, F.; Nordlund, D.; Mecklenburg, M.; Ge, M.Y.; Rong, J.P.; Zhang, A.Y.; Shen, C.F.; Liu, Y.H.; Cao, Y.; et al. Atomic Insights into the Enhanced Surface Stability in High Voltage Cathode Materials by Ultrathin Coating. *Adv. Funct. Mater.* **2017**, *27*, 9. [CrossRef]

37. Guan, D.S.; Jeevarajan, J.A.; Wang, Y. Enhanced cycleability of $LiMn_2O_4$ cathodes by atomic layer deposition of nanosized-thin Al_2O_3 coatings. *Nanoscale* **2011**, *3*, 1465–1469. [CrossRef]

38. Guan, D.S.; Wang, Y. Ultrathin surface coatings to enhance cycling stability of $LiMn_2O_4$ cathode in lithium-ion batteries. *Ionics* **2013**, *19*, 1–8. [CrossRef]

39. Jung, Y.S.; Cavanagh, A.S.; Dillon, A.C.; Groner, M.D.; George, S.M.; Lee, S.H. Enhanced Stability of $LiCoO_2$ Cathodes in Lithium-Ion Batteries Using Surface Modification by Atomic Layer Deposition. *J. Electrochem. Society* **2010**, *157*, A75–A81. [CrossRef]

40. Jung, Y.S.; Cavanagh, A.S.; Riley, L.A.; Kang, S.H.; Dillon, A.C.; Groner, M.D.; George, S.M.; Lee, S.H. Ultrathin Direct Atomic Layer Deposition on Composite Electrodes for Highly Durable and Safe Li-Ion Batteries. *Adv. Mater.* **2010**, *22*, 2172–2176. [CrossRef]

41. Kim, J.W.; Kim, D.H.; Oh, D.Y.; Lee, H.; Kim, J.H.; Lee, J.H.; Jung, Y.S. Surface chemistry of $LiNi_{0.5}Mn_{1.5}O_4$ particles coated by Al_2O_3 using atomic layer deposition for lithium-ion batteries. *J. Power Sources* **2015**, *274*, 1254–1262. [CrossRef]

42. Kim, C.A.; Choi, H.J.; Lee, J.H.; Yoo, S.Y.; Kim, J.W.; Shim, J.H.; Kang, B. Influence of surface modification on electrochemical performance of high voltage spinel ordered-LiNi$_{0.5}$Mn$_{1.5}$O$_4$ exposed to 5.3 V for 100 h before and after surface modification with ALD method. *Electrochim. Acta* **2015**, *184*, 134–142. [CrossRef]

43. Koshtyal, Y.M.; Rumyantsev, A.M.; Maximov, M.Y.; Popovich, A.A.; Zhdanov, V.V. Li$_{1.25}$Ni$_{0.13}$Co$_{0.13}$Mn$_{0.54}$O$_2$ Based Electrodes Modified by Alumina Thin Layers. In Proceedings of the International workshop Atomic Layer Deposition Russia 2015 (ALD Russia 2015), Moscow, Russia, 21–23 September 2015; pp. 65–66.

44. Laskar, M.R.; Jackson, D.H.K.; Xu, S.Z.; Hamers, R.J.; Morgan, D.; Kuech, T.F. Atomic Layer Deposited MgO: A Lower Overpotential Coating for Li[Ni$_{0.5}$Mn$_{0.3}$Co$_{0.2}$]O$_2$ Cathode. *Acs Appl. Mater. Interfaces* **2017**, *9*, 11231–11239. [CrossRef]

45. Li, X.F.; Liu, J.; Meng, X.B.; Tang, Y.J.; Banis, M.N.; Yang, J.L.; Hu, Y.H.; Li, R.Y.; Cai, M.; Sun, X.L. Significant impact on cathode performance of lithium-ion batteries by precisely controlled metal oxide nanocoatings via atomic layer deposition. *J. Power Sources* **2014**, *247*, 57–69. [CrossRef]

46. Luan, X.N.; Guan, D.S.; Wang, Y. Enhancing High-Rate and Elevated-Temperature Performances of Nano-Sized and Micron-Sized LiMn$_2$O$_4$ in Lithium-Ion Batteries with Ultrathin Surface Coatings. *J. Nanosci. Nanotechnol.* **2012**, *12*, 7113–7120. [CrossRef]

47. Mattelaer, F.; Vereecken, P.M.; Dendooven, J.; Detavernier, C. The Influence of Ultrathin Amorphous ALD Alumina and Titania on the Rate Capability of Anatase TiO$_2$ and LiMn$_2$O$_4$ Lithium Ion Battery Electrodes. *Adv. Mater. Interfaces* **2017**, *4*, 11. [CrossRef]

48. Park, J.S.; Meng, X.B.; Elam, J.W.; Hao, S.Q.; Wolverton, C.; Kim, C.; Cabana, J. Ultrathin Lithium-Ion Conducting Coatings for Increased Interfacial Stability in High Voltage Lithium-Ion Batteries. *Chem. Mater.* **2014**, *26*, 3128–3134. [CrossRef]

49. Patel, R.L.; Xie, H.; Park, J.; Asl, H.Y.; Choudhury, A.; Liang, X.H. Significant Capacity and Cycle-Life Improvement of Lithium-Ion Batteries through Ultrathin Conductive Film Stabilized Cathode Particles. *Adv. Mater. Interfaces* **2015**, *2*, 9. [CrossRef]

50. Popovich, A.A.; Maksimov, M.Y.; Rumyantsev, A.M.; Novikov, P.A. Increasing the cyclic life of electrodes based on LiCoO$_2$ used in lithium-ion batteries. *J. App. Chem.* **2015**, *88*, 831–832.

51. Riley, L.A.; Van Ana, S.; Cavanagh, A.S.; Yan, Y.F.; George, S.M.; Liu, P.; Dillon, A.C.; Lee, S.H. Electrochemical effects of ALD surface modification on combustion synthesized LiNi$_{1/3}$Mn$_{1/3}$Co$_{1/3}$O$_2$ as a layered-cathode material. *J. Power Sources* **2011**, *196*, 3317–3324. [CrossRef]

52. Scott, I.D.; Jung, Y.S.; Cavanagh, A.S.; An, Y.F.; Dillon, A.C.; George, S.M.; Lee, S.H. Ultrathin Coatings on Nano-LiCoO$_2$ for Li-Ion Vehicular Applications. *Nano Lett.* **2011**, *11*, 414–418. [CrossRef]

53. Shi, Y.; Zhang, M.H.; Qian, D.N.; Meng, Y.S. Ultrathin Al$_2$O$_3$ Coatings for Improved Cycling Performance and Thermal Stability of LiNi$_{0.5}$Co$_{0.2}$Mn$_{0.3}$O$_2$ Cathode Material. *Electrochim. Acta* **2016**, *203*, 154–161. [CrossRef]

54. Song, J.; Han, X.G.; Gaskell, K.J.; Xu, K.; Lee, S.B.; Hu, L.B. Enhanced electrochemical stability of high-voltage LiNi$_{0.5}$Mn$_{1.5}$O$_4$ cathode by surface modification using atomic layer deposition. *J. Nanoparticle Res.* **2014**, *16*, 8. [CrossRef]

55. Su, Y.T.; Cui, S.H.; Zhuo, Z.Q.; Yang, W.L.; Wang, X.W.; Pan, F. Enhancing the High-Voltage Cycling Performance of LiNi$_{0.5}$Mn$_{0.3}$Co$_{0.2}$O$_2$ by Retarding Its Interfacial Reaction with an Electrolyte by Atomic-Layer-Deposited Al$_2$O$_3$. *Acs Appl. Mater. Interfaces* **2015**, *7*, 25105–25112. [CrossRef]

56. Waller, G.H.; Brooke, P.D.; Rainwater, B.H.; Lai, S.Y.; Hu, R.; Ding, Y.; Alamgir, F.M.; Sandhage, K.H.; Liu, M.L. Structure and surface chemistry of Al$_2$O$_3$ coated LiMn$_2$O$_4$ nanostructured electrodes with improved lifetime. *J. Power Sources* **2016**, *306*, 162–170. [CrossRef]

57. Wise, A.M.; Ban, C.M.; Weker, J.N.; Misra, S.; Cavanagh, A.S.; Wu, Z.C.; Li, Z.; Whittingham, M.S.; Xu, K.; George, S.M.; et al. Effect of Al$_2$O$_3$ Coating on Stabilizing LiNi$_{0.4}$Mn$_{0.4}$Co$_{0.2}$O$_2$ Cathodes. *Chem. Mater.* **2015**, *27*, 6146–6154. [CrossRef]

58. Woo, J.H.; Trevey, J.E.; Cavanagh, A.S.; Choi, Y.S.; Kim, S.C.; George, S.M.; Oh, K.H.; Lee, S.H. Nanoscale Interface Modification of LiCoO$_2$ by Al$_2$O$_3$ Atomic Layer Deposition for Solid-State Li Batteries. *J. Electrochem. Soc.* **2012**, *159*, A1120–A1124. [CrossRef]

59. Woo, J.H.; Travis, J.J.; George, S.M.; Lee, S.H. Utilization of Al$_2$O$_3$ Atomic Layer Deposition for Li Ion Pathways in Solid State Li Batteries. *J. Electrochem. Soc.* **2015**, *162*, A344–A349. [CrossRef]

60. Xiao, X.C.; Ahn, D.; Liu, Z.Y.; Kim, J.H.; Lu, P. Atomic layer coating to mitigate capacity fading associated with manganese dissolution in lithium ion batteries. *Electrochem. Commun.* **2013**, *32*, 31–34. [CrossRef]

61. Xiao, B.W.; Wang, B.Q.; Liu, J.; Kaliyappan, K.; Sun, Q.; Liu, Y.L.; Dadheech, G.; Balogh, M.P.; Yang, L.; Sham, T.K.; et al. Highly stable Li$_{1.2}$Mn$_{0.54}$Co$_{0.13}$Ni$_{0.13}$O$_2$ enabled by novel atomic layer deposited AlPO$_{(4)}$ coating. *Nano Energy* **2017**, *34*, 120–130. [CrossRef]

62. Xie, M.; Li, B.; Zhou, Y. Free-standing high-voltage LiCoO$_2$/multi-wall carbon nanotube paper electrodes with extremely high areal mass loading for lithium ion batteries. *J. Mater. Chem. A* **2015**, *3*, 23180–23184. [CrossRef]

63. Xie, M.; Hu, T.; Yang, L.; Zhou, Y. Synthesis of high-voltage (4.7 V) LiCoO$_2$ cathode materials with Al doping and conformal Al$_2$O$_3$ coating by atomic layer deposition. *Rsc Adv.* **2016**, *6*, 63250–63255. [CrossRef]

64. Yan, P.F.; Zheng, J.M.; Zhang, X.F.; Xu, R.; Amine, K.; Xiao, J.; Zhang, J.G.; Wang, C.M. Atomic to Nanoscale Investigation of Functionalities of an Al$_2$O$_3$ Coating Layer on a Cathode for Enhanced Battery Performance. *Chem. Mater.* **2016**, *28*, 857–863. [CrossRef]

65. Zhang, X.F.; Belharouak, I.; Li, L.; Lei, Y.; Elam, J.W.; Nie, A.M.; Chen, X.Q.; Yassar, R.S.; Axelbaum, R.L. Structural and Electrochemical Study of Al$_2$O$_3$ and TiO$_2$ Coated Li$_{1.2}$Ni$_{0.13}$Mn$_{0.54}$Co$_{0.13}$O$_2$ Cathode Material Using ALD. *Adv. Energy Mater.* **2013**, *3*, 1299–1307. [CrossRef]

66. Zhang, X.F.; Meng, X.B.; Elam, J.W.; Belharouak, I. Electrochemical characterization of voltage fade of Li$_{1.2}$Ni$_{0.2}$Mn$_{0.6}$O$_2$ cathode. *Solid State Ion.* **2014**, *268*, 231–235. [CrossRef]

67. Zhao, J.Q.; Wang, Y. Surface modifications of Li-ion battery electrodes with various ultrathin amphoteric oxide coatings for enhanced cycleability. *J. Solid State Electrochem.* **2013**, *17*, 1049–1058. [CrossRef]

68. Zhao, J.Q.; Aziz, S.; Wang, Y. Hierarchical functional layers on high-capacity lithium-excess cathodes for superior lithium ion batteries. *J. Power Sources* **2014**, *247*, 95–104. [CrossRef]

69. Zhou, Y.; Lee, Y.H.; Sun, H.X.; Wallas, J.M.; George, S.M.; Xie, M. Coating Solution for High-Voltage Cathode: AlF_3 Atomic Layer Deposition for Freestanding $LiCoO_2$ Electrodes with High Energy Density and Excellent Flexibility. *Acs Appl. Mater. Interfaces* **2017**, *9*, 9614–9619. [CrossRef]

70. Jung, Y.S.; Cavanagh, A.S.; Yan, Y.F.; George, S.M.; Manthiram, A. Effects of Atomic Layer Deposition of Al_2O_3 on the Li $Li_{0.20}Mn_{0.54}Ni_{0.13}Co_{0.13}O_2$ Cathode for Lithium-Ion Batteries. *J. Electrochem. Soc.* **2011**, *158*, A1298–A1302. [CrossRef]

71. Kim, J.W.; Travis, J.J.; Hu, E.Y.; Nam, K.W.; Kim, S.C.; Kang, C.S.; Woo, J.H.; Yang, X.Q.; George, S.M.; Oh, K.H.; et al. Unexpected high power performance of atomic layer deposition coated Li $Ni_{1/3}Mn_{1/3}Co_{1/3}O_2$ cathodes. *J. Power Sources* **2014**, *254*, 190–197. [CrossRef]

72. Shi, Y.; Xing, Y.; Kim, K.; Yu, T.; Lipson, A.L.; Dameron, A.; Connell, J.G. Communication—Reduction of DC Resistance of Ni-Rich Lithium Transition Metal Oxide Cathode by Atomic Layer Deposition. *J. Electrochem. Soc.* **2021**, *168*, 040501. [CrossRef]

73. Tesfamhret, Y.; Liu, H.; Chai, Z.; Berg, E.; Younesi, R. On the Manganese Dissolution Process from $LiMn_2O_4$ Cathode Materials. *ChemElectroChem* **2021**, *8*, 1516–1523. [CrossRef]

74. Wang, X.; Cai, J.; Liu, Y.; Han, X.; Ren, Y.; Li, J.; Liu, Y.; Meng, X. Atomic-scale Constituting Stable Interface for Improved $LiNi_{0.6}Mn_{0.2}Co_{0.2}O_2$ Cathodes of Lithium-ion Batteries. *Nanotechnology* **2020**, *32*, 115401. [CrossRef]

75. Kim, D.; Park, D.; Ko, C.H.; Shin, K.; Lee, Y.-S. Improving Electrochemical Performance of Ni-rich Cathode Using Atomic Layer Deposition with Particle by Particle Coating Method. *J. Electrochem. Sci. Technol.* **2021**, *12*, 237–245. [CrossRef]

76. Chen, Y.; Wang, M.; Chen, J.; Yang, J.; Li, Z.; Huang, Y.; Chen, Z.; Zou, Y.; Zheng, J.; Li, X. Atomic layer deposition of Al_2O_3 on $LiNi_{0.68}Co_{0.10}Mn_{0.22}O_2$ for enhanced electrochemical performance. *Mater. Lett.* **2020**, *271*, 127771. [CrossRef]

77. Zhisen, Z.; Gao, D.; Yang, G.; Wu, Q.; Ren, X.; Zhang, P.; Li, Y. Ultrathin interfacial modification of Li-rich layered oxide electrode/sulfide solid electrolyte via atomic layer deposition for high electrochemical performance battery. *Nanotechnology* **2020**, *31*, 454001. [CrossRef]

78. Zhou, M. Structural and Electrochemical Properties of $Li_{1.2}Ni_{0.16}Mn_{0.54}Co_{0.08}O_2$—$Al_2O_3$ Composite Prepared by Atomic Layer Deposition as the Cathode Material for LIBs. *Int. J. Electrochem. Science* **2020**, 10759–10771. [CrossRef]

79. Evenstein, E.; Rosy; Haber, S.; Sclar, H.; Houben, L.; Leung, K.; Leskes, M.; Noked, M. Atomic surface reduction of interfaces utilizing vapor phase approach: High energy $LiNixMnyCoz$ oxide as a test case. *Energy Storage Mater.* **2019**, *19*, 261–269. [CrossRef]

80. Han, B.; Key, B.; Lipton, A.S.; Vaughey, J.T.; Hughes, B.; Trevey, J.; Dogan, F. Influence of Coating Protocols on Alumina-Coated Cathode Material: Atomic Layer Deposition versus Wet-Chemical Coating. *J. Electrochem. Soc.* **2019**, *166*, A3679–A3684. [CrossRef]

81. Hoskins, A.L.; McNeary, W.W.; Millican, S.L.; Gossett, T.A.; Lai, A.; Gao, Y.; Liang, X.; Musgrave, C.B.; Weimer, A.W. Nonuniform Growth of Sub-2 Nanometer Atomic Layer Deposited Alumina Films on Lithium Nickel Manganese Cobalt Oxide Cathode Battery Materials. *ACS Appl. Nano Mater.* **2019**, *2*, 6989–6997. [CrossRef]

82. Huang, B.; Wang, R.; Gong, Y.; He, B.; Wang, H. Enhanced Cycling Stability of Cation Disordered Rock-Salt $Li_{(1.2)}Ti_{(0.4)}Mn_{(0.4)}O_{(2)}$ Material by Surface Modification With $Al_{(2)}O_{(3)}$. *Front. Chem.* **2019**, *7*, 107. [CrossRef]

83. Jurng, S.; Heiskanen, S.K.; Chandrasiri, K.W.D.K.; Abeywardana, M.Y.; Lucht, B.L. Minimized Metal Dissolution from High-Energy Nickel Cobalt Manganese Oxide Cathodes with Al_2O_3 Coating and Its Effects on Electrolyte Decomposition on Graphite Anodes. *J. Electrochem. Soc.* **2019**, *166*, A2721–A2726. [CrossRef]

84. Seung-Hyun Lee, D.; Im, W.B.; Liang, X. High density conductive $LiFePO_4$ cathode with enhanced high-rate and high temperature performance. *Mater. Chem. Phys.* **2019**, *232*, 367–373. [CrossRef]

85. Neudeck, S.; Mazilkin, A.; Reitz, C.; Hartmann, P.; Janek, J.; Brezesinski, T. Effect of Low-Temperature Al_2O_3 ALD Coating on Ni-Rich Layered Oxide Composite Cathode on the Long-Term Cycling Performance of Lithium-Ion Batteries. *Sci. Rep.* **2019**, *9*, 5328. [CrossRef] [PubMed]

86. Ramasamy, H.; Sinha, S.; Park, J.; Gong, M.; Aravindan, V.; Heo, J.; Lee, Y.-S. Enhancement of Electrochemical Activity of Ni-rich $LiNi_{0.8}Mn_{0.1}Co_{0.1}O_2$ by Precisely Controlled Al_2O_3 Nanocoatings via Atomic Layer Deposition. *J. Electrochem. Sci. Technol.* **2019**, *10*, 196–205. [CrossRef]

87. Yu, H.; Gao, Y.; Liang, X. Slightly Fluorination of Al_2O_3 ALD Coating on $Li_{1.2}Mn_{0.54}Co_{0.13}Ni_{0.13}O_2$ Electrodes: Interface Reaction to Create Stable Solid Permeable Interphase Layer. *J. Electrochem. Soc.* **2019**, *166*, A2021–A2027. [CrossRef]

88. Zhu, W.; Huang, X.; Liu, T.; Xie, Z.; Wang, Y.; Tian, K.; Bu, L.; Wang, H.; Gao, L.; Zhao, J. Ultrathin Al_2O_3 Coating on $LiNi_{0.8}Co_{0.1}Mn_{0.1}O_2$ Cathode Material for Enhanced Cycleability at Extended Voltage Ranges. *Coatings* **2019**, *9*, 92. [CrossRef]

89. Gao, Y.; Park, J.; Liang, X. Synergic Titanium Nitride Coating and Titanium Doping by Atomic Layer Deposition for Stable- and High-Performance Li-Ion Battery. *J. Electrochem. Soc.* **2018**, *165*, A3871–A3877. [CrossRef]

90. Østli, E.R.; Tesfamhret, Y.; Wenner, S.; Lacey, M.J.; Brandell, D.; Svensson, A.M.; Selbach, S.M.; Wagner, N.P. Limitations of Ultrathin Al_2O_3 Coatings on LNMO Cathodes. *ACS Omega* **2021**, *6*, 30644–30655. [CrossRef]

91. Jackson, D.H.K.; Kuech, T.F. Electrochemical effects of annealing on atomic layer deposited Al_2O_3 coatings on $LiNi_{0.5}Mn_{0.3}Co_{0.2}O_2$. *J. Power Sources* **2017**, *365*, 61–67. [CrossRef]

92. Young, M.J.; Letourneau, S.; Warburton, R.E.; Dose, W.M.; Johnson, C.; Greeley, J.; Elam, J.W. High-Rate Spinel LiMn$_2$O$_4$ (LMO) Following Carbonate Removal and Formation of Li-Rich Interface by ALD Treatment. *J. Phys. Chem. C* **2019**, *123*, 23783–23790. [CrossRef]

93. David, L.; Dahlberg, K.; Mohanty, D.; Ruther, R.E.; Huq, A.; Chi, M.; An, S.J.; Mao, C.; King, D.M.; Stevenson, L.; et al. Unveiling the Role of Al$_2$O$_3$ in Preventing Surface Reconstruction During High-Voltage Cycling of Lithium-Ion Batteries. *ACS Appl. Energ. Mater.* **2019**, *2*, 1308–1313. [CrossRef]

94. Haridas, A.K.; Nguyen, Q.A.; Song, B.F.; Blaser, R.; Biswal, S.L. ALD-Modified LiNi$_{0.33}$Mn$_{0.33}$Co$_{0.33}$O$_2$ Paired with Macroporous Silicon for Lithium-Ion Batteries: An Investigation on Lithium Trapping, Resistance Rise, and Cycle-Life Performance. *ACS Appl. Energ. Mater.* **2020**, *3*, 456–468. [CrossRef]

95. He, Y.; Pham, H.; Gao, Y.; Patel, R.L.; Sarkar, S.; Liang, X.; Park, J. Discovery of an Unexpected Metal Dissolution of Thin-Coated Cathode Particles and Its Theoretical Explanation. *Adv. Theory Simul.* **2020**, *3*, 2000002. [CrossRef]

96. Warburton, R.E.; Young, M.J.; Letourneau, S.; Elam, J.W.; Greeley, J. Descriptor-Based Analysis of Atomic Layer Deposition Mechanisms on Spinel LiMn$_2$O$_4$ Lithium-Ion Battery Cathodes. *Chem. Mater.* **2020**, *32*, 1794–1806. [CrossRef]

97. Negi, R.S.; Culver, S.P.; Wiche, M.; Ahmed, S.; Volz, K.; Elm, M.T. Optimized atomic layer deposition of homogeneous, conductive Al$_2$O$_3$ coatings for high-nickel NCM containing ready-to-use electrodes. *Phys. Chem. Chem. Phys.* **2021**, *23*, 6725–6737. [CrossRef]

98. Laskar, M.R.; Jackson, D.H.K.; Guan, Y.X.; Xu, S.Z.; Fang, S.Y.; Dreibelbis, M.; Mahanthappa, M.K.; Morgan, D.; Hamers, R.J.; Kuech, T.F. Atomic Layer Deposition of Al$_2$O$_3$-Ga$_2$O$_3$ Alloy Coatings for LiNi$_{0.5}$Mn$_{0.3}$Co$_{0.2}$O$_2$ Cathode to Improve Rate Performance in Li-Ion Battery. *Acs Appl. Mater. Interfaces* **2016**, *8*, 10572–10580. [CrossRef]

99. Jackson, D.H.K.; Laskar, M.R.; Fang, S.Y.; Xu, S.Z.; Ellis, R.G.; Li, X.Q.; Dreibelbis, M.; Babcock, S.E.; Mahanthappa, M.K.; Morgan, D.; et al. Optimizing AlF$_3$ atomic layer deposition using trimethylaluminum and TaF5: Application to high voltage Li-ion battery cathodes. *J. Vac. Sci. Technol. A* **2016**, *34*, 8. [CrossRef]

100. Shapira, A.; Tiurin, O.; Solomatin, N.; Auinat, M.; Meitav, A.; Ein-Eli, Y. Robust AlF3 Atomic Layer Deposition Protective Coating on LiMn$_{1.5}$Ni$_{0.5}$O$_4$ Particles: An Advanced Li-Ion Battery Cathode Material Powder. *ACS Appl. Energ. Mater.* **2018**, *1*, 6809–6823. [CrossRef]

101. Deng, S.; Xiao, B.; Wang, B.; Li, X.; Kaliyappan, K.; Zhao, Y.; Lushington, A.; Li, R.; Sham, T.-K.; Wang, H.; et al. New insight into atomic-scale engineering of electrode surface for long-life and safe high voltage lithium ion cathodes. *Nano Energy* **2017**, *38*, 19–27. [CrossRef]

102. Henderick, L.; Hamed, H.; Mattelaer, F.; Minjauw, M.; Meersschaut, J.; Dendooven, J.; Safari, M.; Vereecken, P.; Detavernier, C. Atomic Layer Deposition of Nitrogen-Doped Al Phosphate Coatings for Li-Ion Battery Applications. *ACS Appl. Mater. Interfaces* **2020**, *12*, 25949–25960. [CrossRef]

103. Park, J.S.; Mane, A.U.; Elam, J.W.; Croy, J.R. Amorphous Metal Fluoride Passivation Coatings Prepared by Atomic Layer Deposition on LiCoO$_2$ for Li-Ion Batteries. *Chem. Mater.* **2015**, *27*, 1917–1920. [CrossRef]

104. Patel, R.L.; Palaparty, S.A.; Liang, X.H. Ultrathin Conductive CeO$_2$ Coating for Significant Improvement in Electrochemical Performance of LiMn1.5Ni0.5O4 Cathode Materials. *J. Electrochem. Soc.* **2017**, *164*, A6236–A6243. [CrossRef]

105. Sarkar, S.; Patel, R.L.; Liang, X.; Park, J. Unveiling the Role of CeO$_2$ Atomic Layer Deposition Coatings on LiMn$_2$O$_4$ Cathode Materials: An Experimental and Theoretical Study. *ACS Appl. Mater. Interfaces* **2017**, *9*, 30599–30607. [CrossRef]

106. Sarkar, S.; Patel, R.; Liang, X.; Park, J. A Comprehensive Understanding on How Ultrathin Coating Layers on Active Particles Enhance Battery Performance Significantly. *ECS Trans.* **2017**, *77*, 425–436. [CrossRef]

107. Patel, R.L.; Jiang, Y.B.; Choudhury, A.; Liang, X.H. Employing Synergetic Effect of Doping and Thin Film Coating to Boost the Performance of Lithium-Ion Battery Cathode Particles. *Sci. Rep.* **2016**, *6*, 11. [CrossRef]

108. Gao, Y.; He, X.; Ma, L.; Wu, T.; Park, J.; Liang, X. Understanding cation doping achieved by atomic layer deposition for high-performance Li-Ion batteries. *Electrochim. Acta* **2020**, *340*, 135951. [CrossRef]

109. Gao, Y.; Shang, Z.; He, X.; White, T.; Park, J.; Liang, X. Cooperating effects of conformal iron oxide (FeO$_x$) ALD coating and post-annealing on Li-Rich layered cathode materials. *Electrochim. Acta* **2019**, *318*, 513–524. [CrossRef]

110. Gao, Y.; Yu, H.; Sandineni, P.; He, X.; Choudhury, A.; Park, J.; Liang, X. Fe Doping in LiMn$_{1.5}$Ni$_{0.5}$O$_4$ by Atomic Layer Deposition Followed by Annealing: Depths and Occupation Sites. *J. Phys. Chem. C* **2021**, *125*, 7560–7567. [CrossRef]

111. Xiao, B.W.; Liu, J.; Sun, Q.; Wang, B.Q.; Banis, M.N.; Zhao, D.; Wang, Z.Q.; Li, R.Y.; Cui, X.Y.; Sham, T.K.; et al. Unravelling the Role of Electrochemically Active FePO$_4$ Coating by Atomic Layer Deposition for Increased High-Voltage Stability of LiNi$_{0.5}$Mn$_{1.5}$O$_4$ Cathode Material. *Adv. Sci.* **2015**, *2*, 6. [CrossRef] [PubMed]

112. Kitsche, D.; Tang, Y.; Ma, Y.; Goonetilleke, D.; Sann, J.; Walther, F.; Bianchini, M.; Janek, J.; Brezesinski, T. High Performance All-Solid-State Batteries with a Ni-Rich NCM Cathode Coated by Atomic Layer Deposition and Lithium Thiophosphate Solid Electrolyte. *ACS Appl. Energ. Mater.* **2021**, *4*, 7338–7345. [CrossRef]

113. Tiurin, O.; Solomatin, N.; Auinat, M.; Ein-Eli, Y. Atomic layer deposition (ALD) of lithium fluoride (LiF) protective film on Li-ion battery LiMn$_{1.5}$Ni$_{0.5}$O$_4$ cathode powder material. *J. Power Sources* **2020**, *448*, 227373. [CrossRef]

114. Hallot, M.; Caja-Munoz, B.; Leviel, C.; Lebedev, O.I.; Retoux, R.; Avila, J.; Roussel, P.; Asensio, M.C.; Lethien, C. Atomic Layer Deposition of a Nanometer-Thick Li$_3$PO$_4$ Protective Layer on LiNi0.5Mn1.5O4 Films: Dream or Reality for Long-Term Cycling? *ACS Appl. Mater. Interfaces* **2021**, *13*, 15761–15773. [CrossRef]

115. Li, X.F.; Liu, J.; Banis, M.N.; Lushington, A.; Li, R.Y.; Cai, M.; Sun, X.L. Atomic layer deposition of solid-state electrolyte coated cathode materials with superior high-voltage cycling behavior for lithium ion battery application. *Energy Environ. Sci.* **2014**, *7*, 768–778. [CrossRef]

116. Wang, E.; Zhao, Y.; Xiao, D.; Zhang, X.; Wu, T.; Wang, B.; Zubair, M.; Li, Y.; Sun, X.; Yu, H. Composite Nanostructure Construction on the Grain Surface of Li-Rich Layered Oxides. *Adv. Mater.* **2020**, *32*, 1906070. [CrossRef]

117. Ahaliabadeh, Z.; Miikkulainen, V.; Mäntymäki, M.; Mousavihashemi, S.; Lahtinen, J.; Lide, Y.; Jiang, H.; Mizohata, K.; Kankaanpää, T.; Kallio, T. Understanding the Stabilizing Effects of Nanoscale Metal Oxide and Li–Metal Oxide Coatings on Lithium-Ion Battery Positive Electrode Materials. *ACS Appl. Mater. Interfaces* **2021**, *13*, 42773–42790. [CrossRef]

118. Kraytsberg, A.; Drezner, H.; Auinat, M.; Shapira, A.; Solomatin, N.; Axmann, P.; Wohlfahrt-Mehrens, M.; Ein-Eli, Y. Atomic Layer Deposition of a Particularized Protective MgF_2 Film on a Li-Ion Battery $LiMn_{1.5}Ni_{0.5}O_4$ Cathode Powder Material. *ChemNanoMat* **2015**, *1*, 577–585. [CrossRef]

119. Aribia, A.; Sastre, J.; Chen, X.; Gilshtein, E.; Futscher, M.; Tiwari, A.; Romanyuk, Y. In Situ Lithiated ALD Niobium Oxide for Improved Long Term Cycling of Layered Oxide Cathodes:A Thin-Film Model Study. *J. Electrochem. Soc.* **2021**, *168*, 040513. [CrossRef]

120. Su, Y.; Gu, D.; Shao, Y.; Wang, X.; Pan, F. Improved electrochemical performance of $LiNi_{0.5}Mn_{0.3}Co_{0.2}O_2$ electrodes coated by atomic-layer-deposited Ta_2O_5. *Funct. Mater. Lett.* **2018**, *12*, 1850103. [CrossRef]

121. Qin, C.C.; Cao, J.L.; Chen, J.; Dai, G.L.; Wu, T.F.; Chen, Y.B.; Tang, Y.F.; Li, A.D.; Chen, Y.F. Improvement of electrochemical performance of nickel rich $LiNi_{0.6}Co_{0.2}Mn_{0.2}O_2$ cathode active material by ultrathin TiO_2 coating. *Dalton Trans.* **2016**, *45*, 9669–9675. [CrossRef]

122. Wang, C.-C.; Lin, J.-W.; Yu, Y.-H.; Lai, K.-H.; Chiu, K.-F.; Kei, C.-C. Electrochemical and Structural Investigation on Ultrathin ALD ZnO and TiO_2 Coated Lithium-Rich Layered Oxide Cathodes. *ACS Sustain. Chem. Eng.* **2018**, *6*, 16941–16950. [CrossRef]

123. Zhang, C.; Su, J.; Wang, T.; Yuan, K.; Chunguag, C.; Liu, S.; Huang, T.; Wu, J.-H.; Lu, H.; Yu, A. Significant Improvement on Electrochemical Performance of $LiMn_2O_4$ at Elevated Temperature by Atomic Layer Deposition of TiO_2 Nanocoating. *ACS Sustain. Chem. Eng.* **2018**, *6*, 7890–7901. [CrossRef]

124. Hsieh, C.-T.; Chao, C.-H.; Ke, W.-J.; Lin, Y.-F.; Liu, H.-W.; Gandomi, Y.A.; Gu, S.; Su, C.-Y.; Chang, J.-K.; Li, J.; et al. Roll-To-Roll Atomic Layer Deposition of Titania Nanocoating on Thermally Stabilizing Lithium Nickel Cobalt Manganese Oxide Cathodes for Lithium Ion Batteries. *ACS Appl. Energ. Mater.* **2020**, *3*, 10619–10631. [CrossRef]

125. Wang, C.-C.; Lin, J.-W.; Yu, Y.-H.; Lai, K.-H.; Lee, S.-M.; Chiu, K.-F.; Kei, C.-C. Nanolaminated ZnO–TiO_2 coated lithium-rich layered oxide cathodes by atomic layer deposition for enhanced electrochemical performances. *J. Alloy. Compd.* **2020**, *842*, 155845. [CrossRef]

126. Deng, S.; Wang, B.; Yuan, Y.; Li, X.; Sun, Q.; Doyle-Davis, K.; Banis, M.N.; Liang, J.; Zhao, Y.; Li, J.; et al. Manipulation of an ionic and electronic conductive interface for highly-stable high-voltage cathodes. *Nano Energy* **2019**, *65*, 103988. [CrossRef]

127. Henderick, L.; Hamed, H.; Mattelaer, F.; Minjauw, M.; Nisula, M.; Meersschaut, J.; Dendooven, J.; Safari, M.; Vereecken, P.; Detavernier, C. Plasma enhanced atomic layer deposition of a (nitrogen doped) Ti phosphate coating for improved energy storage in Li-ion batteries. *J. Power Sources* **2021**, *497*, 229866. [CrossRef]

128. Prasadam, V.P.; Bahlawane, N.; Mattelaer, F.; Rampelberg, G.; Detavernier, C.; Fang, L.; Jiang, Y.; Martens, K.; Parkin, I.P.; Papakonstantinou, I. Atomic layer deposition of vanadium oxides: Process and application review. *Mater. Today Chem.* **2019**, *12*, 396–423. [CrossRef]

129. Aziz, S.; Zhao, J.Q.; Cain, C.; Wang, Y. Nanoarchitectured $LiMn_2O_4$/Graphene/ZnO Composites as Electrodes for Lithium Ion Batteries. *J. Mater. Sci. Technol.* **2014**, *30*, 427–433. [CrossRef]

130. Kong, J.Z.; Ren, C.; Tai, G.A.; Zhang, X.; Li, A.D.; Wu, D.; Li, H.; Zhou, F. Ultrathin ZnO coating for improved electrochemical performance of $LiNi_{0.5}Co_{0.2}Mn_{0.3}O_2$ cathode material. *J. Power Sources* **2014**, *266*, 433–439. [CrossRef]

131. Zhao, J.Q.; Wang, Y. Ultrathin Surface Coatings for Improved Electrochemical Performance of Lithium Ion Battery Electrodes at Elevated Temperature. *J. Phys. Chem. C* **2012**, *116*, 11867–11876. [CrossRef]

132. Kong, J.Z.; Wang, S.S.; Tai, G.A.; Zhu, L.; Wang, L.G.; Zhai, H.F.; Wu, D.; Li, A.D.; Li, H. Enhanced electrochemical performance of $LiNi_{0.5}Co_{0.2}Mn_{0.3}O_2$ cathode material by ultrathin ZrO_2 coating. *J. Alloy. Compd.* **2016**, *657*, 593–600. [CrossRef]

133. Zhao, J.Q.; Qu, G.Y.; Flake, J.C.; Wang, Y. Low temperature preparation of crystalline ZrO_2 coatings for improved elevated-temperature performances of Li-ion battery cathodes. *Chem. Commun.* **2012**, *48*, 8108–8110. [CrossRef] [PubMed]

134. Zhao, J.Q.; Wang, Y. Atomic layer deposition of epitaxial ZrO_2 coating on $LiMn_2O_4$ nanoparticles for high-rate lithium ion batteries at elevated temperature. *Nano Energy* **2013**, *2*, 882–889. [CrossRef]

135. Liu, Y.; Wang, X.; Cai, J.; Han, X.; Geng, D.; Li, J.; Meng, X. Atomic-scale tuned interface of nickel-rich cathode for enhanced electrochemical performance in lithium-ion batteries. *J. Mater. Sci. Technol.* **2020**, *54*, 77–86. [CrossRef]

136. Bao, W.; Qian, G.; Zhao, L.; Yu, Y.; Su, L.; Cai, X.; Zhao, H.; Zuo, Y.; Zhang, Y.; Li, H.; et al. Simultaneous Enhancement of Interfacial Stability and Kinetics of Single-Crystal $LiNi_{0.6}Mn_{0.2}Co_{0.2}O_2$ through Optimized Surface Coating and Doping. *Nano Letters* **2020**, *20*, 8832–8840. [CrossRef] [PubMed]

137. Comstock, D.J.; Elam, J.W. Mechanistic Study of Lithium Aluminum Oxide Atomic Layer Deposition. *Journal of Physical Chemistry C* **2013**, *117*, 1677–1683. [CrossRef]

138. Lee, Y.; DuMont, J.W.; Cavanagh, A.S.; George, S.M. Atomic Layer Deposition of AlF_3 Using Trimethylaluminum and Hydrogen Fluoride. *J. Phys. Chem. C* **2015**, *119*, 14185–14194. [CrossRef]

139. Xing, W. High Energy Density Li-Ion Batteries with ALD Multi-Functional Modified LiCoO$_2$ Cathode. *ECS Trans.* **2017**, *80*, 55–63. [CrossRef]

140. Tiurin, O.; Ein-Eli, Y. A Critical Review: The Impact of the Battery Electrode Material Substrate on the Composition and Properties of Atomic Layer Deposition (ALD) Coatings. *Adv. Mater. Interfaces* **2019**, *6*, 1901455. [CrossRef]

141. Liu, Y.; Hudak, N.S.; Huber, D.L.; Limmer, S.J.; Sullivan, J.P.; Huang, J.Y. In Situ Transmission Electron Microscopy Observation of Pulverization of Aluminum Nanowires and Evolution of the Thin Surface Al$_2$O$_3$ Layers during Lithiation-Delithiation Cycles. *Nano Lett.* **2011**, *11*, 4188–4194. [CrossRef]

142. Tebbe, J.L.; Holder, A.M.; Musgrave, C.B. Mechanisms of LiCoO$_2$ Cathode Degradation by Reaction with HF and Protection by Thin Oxide Coatings. *Acs Appl. Mater. Interfaces* **2015**, *7*, 24265–24278. [CrossRef]

143. Seid, K.A.; Badot, J.C.; Dubrunfaut, O.; Caldes, M.T.; Stephant, N.; Gautier, L.; Guyomard, D.; Lestriez, B. Multiscale electronic transport in Li$_{1+x}$Ni$_{1/3-u}$Co$_{1/3-v}$Mn$_{1/3-w}$O$_2$: A broadband dielectric study from 40 Hz to 10 GHz. *Phys. Chem. Chem. Phys.* **2013**, *15*, 19790–19798. [CrossRef]

144. Tatsuo, N. Express Charging/Discharging Lithium Ion Secondary Batteries. *Tech. News* **2008**, *11*, 3–18.

145. Guo, W.; Zhang, C.; Zhang, Y.; Lin, L.; He, W.; Xie, Q.; Sa, B.; Wang, L.; Peng, D.-L. A Universal Strategy toward the Precise Regulation of Initial Coulombic Efficiency of Li-Rich Mn-Based Cathode Materials. *Adv. Mater.* **2021**, *33*, 2103173. [CrossRef]

146. Li, J.; Li, S.; Xu, S.; Huang, S.; Zhu, J. Synthesis and Electrochemical Properties of LiNi$_{(0.5)}$Mn$_{(1.5)}$O$_{(4)}$ Cathode Materials with Cr$^{(3+)}$ and F$^{(−)}$ Composite Doping for Lithium-Ion Batteries. *Nanoscale Res. Lett.* **2017**, *12*, 414. [CrossRef]

147. Lappalainen, J.; Tuller, H.L.; Lantto, V. Electronic Conductivity and Dielectric Properties of Nanocrystalline CeO$_2$ Films. *J. Electroceram.* **2004**, *13*, 129–133. [CrossRef]

148. Sarah, M.; Musa, M.; Asiah, M.; Rusop, M. Electrical conductivity characteristics of TiO$_2$ thin film. In Proceedings of the 2010 International Conference on Electronic Devices, Systems and Applications, ICEDSA 2010—Proceedings, Kuala Lumpur, Malaysia, 11–14 April 2010. [CrossRef]

149. Caglar, M.; Ilican, S.; Caglar, Y.; Yakuphanoglu, F. Electrical conductivity and optical properties of ZnO nanostructured thin film. *Appl. Surf. Sci.* **2009**, *255*, 4491–4496. [CrossRef]

150. Kuo, D.H.; Chien, C.H.; Huang, C.H. Zirconia and zirconia–silica thin films deposited by magnetron sputtering. *Thin Solid Film.* **2002**, *420–421*, 47–53. [CrossRef]

151. Park, J.S.; Mane, A.U.; Elam, J.W.; Croy, J.R. Atomic Layer Deposition of Al–W–Fluoride on LiCoO$_2$ Cathodes: Comparison of Particle- and Electrode-Level Coatings. *ACS Omega* **2017**, *2*, 3724–3729. [CrossRef]

152. Riyanto, E.; Martides, E.; Pikra, G.; Atmaja, T.D.; Pramana, R.I.; Purwanto, A.J.; Santosa, A.; Junianto, E.; Darussalam, R.; Saepudin, A.; et al. A review of atomic layer deposition for high lithium-ion battery performance. *J. Mater. Res. Technol.* **2021**, *15*, 5466–5481. [CrossRef]

153. Wu, K.; Li, W.; Qin, J.; Hao, Y.; Kheimeh Sari, H.M.; Feng, H.; Li, X. Controllable atomic layer deposition coatings to boost the performance of LiMn$_x$Co$_y$Ni$_{1−x−y}$O$_2$ in lithium-ion batteries: A review. *J. Mater. Res.* **2020**, *35*, 762–774. [CrossRef]